

Structural Shape and Topology Optimization Using an Implicit Free Boundary Parametrization Method

S.Y. Wang^{1,2} and M.Y. Wang³

Abstract: In this paper, an implicit free boundary parametrization method is presented as an effective approach for simultaneous shape and topology optimization of structures. The moving free boundary of a structure is embedded as a zero level set of a higher dimensional implicit level set function. The radial basis functions (RBFs) are introduced to parametrize the implicit function with a high level of accuracy and smoothness. The motion of the free boundary is thus governed by a mathematically more convenient ordinary differential equation (ODE). Eigenvalue stability can be guaranteed due to the use of inverse multiquadric RBF splines. To perform both shape and topology optimization, the steepest gradient method is used to determine a velocity function. To guarantee that the optimal solution be in the feasible domain, a bi-sectioning algorithm is proposed to obtain the Lagrange multiplier. The velocity function is extended in a physically meaningful way and its discontinuity at the free boundary is eliminated by using a smoothing filter. The usual periodic reinitialization process is avoided to allow for the nucleation of new holes. It is shown that simultaneous shape and topology optimization can be obtained and a mass-conservative stable evolution guaranteed due to the present extension velocities. The proposed method is implemented in the framework of classical minimum compliance design and its efficiency and accuracy over the existing methods are highlighted. Numerical examples can demonstrate its excellence in accuracy, convergence speed and insensitivity to initial designs in structural shape and topology optimization of two dimensional (2D) problems.

keyword: Topology optimization, shape optimization, level set method, radial basis functions, gradient method.

1 Introduction

Structural shape and topology optimization has become an effective design tool for obtaining more efficient and lighter structures. A structural optimum topology can be arrived at by the optimal modifications of holes and connectivities of the structural design domain, which is actually implemented by redistributing material in an iterative and systematic manner [Akin and Arjona-Baez (2001); Bendsøe and Kikuchi (1988); Wang and Tai (2004)]. The topology optimization as a conceptual design tool has the highest importance in the developing process of all structural optimization methods because of its ability in achieving greatest savings [Rozvany (2001); Bendsøe and Kikuchi (1988); Xie and Steven (1993); Wang, Tai, and Wang (2006); Wang and Wang (2005c)]. Topology optimization is even regarded as the best method for solving the structural optimal design problem and for producing the best overall structure [Tanskanen (2002)]. The shape optimization changes the surface geometry in a manner that a homogenous stress distribution is achieved. Usually, further improvements due to the shape optimization is only possible with a great effort with respect to time and costs. Structural shape and topology optimization has been identified as one of the most challenging task in structural design [Bendsøe and Sigmund (2003)].

Recently, the level set methods, first introduced by Osher and Sethian in [Osher and Sethian (1988)], have been applied to structural shape and topology optimization problems as an emerging and promising family of methods based on the moving free boundaries [Sethian and Wiegmann (2000); Allaire, Jouve, and Toader (2004); Wang, Wang, and Guo (2003); Wang and Wang (2004a)]. The level set method itself is a simple and versatile method for computing and analyzing the motion of an interface in two or three dimensions and following the evolution of interfaces [Sethian (1999); Osher and Fedkiw (2002)]. Since these interfaces may easily develop sharp corners, break apart, merge together and even disappear

¹ Corresponding author, Email: smaws@nus.edu.sg.

² Centre for Singapore-MIT Alliance, National University of Singapore, E4-04-10, 4 Engineering Drive 3, Singapore 117576.

³ Department of Automation and Computer-Aided Engineering, The Chinese University of Hong Kong, Shatin, NT, Hong Kong.

in a robust and stable manner, both shape and topological changes in the structural design domain can be obtained by taking the voids as a phase and the free boundary as the dynamic interface and thus the level set method can also be used in structural shape and topology optimization as a free boundary-based alternative approach to the conventional element-based structural optimization methods such as the homogeneous approach first proposed by Bendsøe and Kikuchi [Bendsøe and Kikuchi (1988)] or its alternative the SIMP (Solid Isotropic Microstructure with Penalization) method [Bendsøe (1989); Rozvany, Zhou, and Birker (1992)].

Sethian and Wiegmann [Sethian and Wiegmann (2000)] are among the first researchers to extend the level set method of Osher and Sethian [Osher and Sethian (1988)] to capture the free boundary of a structure on a fixed Eulerian mesh. The Von Mises equivalent stress, rather than the more appropriate shape sensitivity, was employed to improve the structural rigidity within the context of 2D linear elasticity using the immersed interface method. Osher and Santosa [Osher and Santosa (2001)] investigated a two-phase optimization of a membrane modeled by a linear scalar partial differential equation. The free boundary was defined as the dynamic interface between two constituents occupying a given design domain. The level set method was combined with the shape sensitivity analysis framework, but without the context of linear or nonlinear elasticity. Wang, Wang and Guo [Wang, Wang, and Guo (2003)] constructed the level set speed (or velocity) function in terms of the shape of the boundary and the variational sensitivity as a physically meaningful link between the general structural topology optimization process and the powerful level set methods. It was also suggested that using the level set methods for structural topology optimization has the promising potentials in flexibility of handling topological changes, fidelity of boundary representation and degree of automation. The level set methods were further developed as a natural setting to combine the rigorous shape variations into the conventional structural topology optimization process in [Wang and Wang (2004a)]. Allaire, Jouve and Toader [Allaire, Jouve, and Toader (2004)] also proposed an implementation of the level-set methods for structural topology optimization where the front velocity during the optimization process was derived from the classical shape sensitivity analysis by using an adjoint method and the front propagation was performed by solv-

ing the Hamilton-Jacobi equation. Furthermore, it was shown that the final solution may strongly depend on the initial design, though drastic topology changes during the structural optimization process were allowed for. In a multi-material design domain, the conventional level set methods have been further developed in [Wang and Wang (2004b)] as a “color level set” method to address the problem of structural shape and topology optimization. An implicit function vector was used to represent different material phases more efficiently to avoid the problem of overlap between material phases of a conventional partitioning approach. In [Wang and Wang (2005b)], the conventional level set methods were further extended to a level set-based variational approach for the optimal shape and topology design of heterogeneous objects using the multi-phase level set model in [Vese and Chan (2002)] for digital image processing, in which the promising features such as strong regularity in the problem formulation and inherent capabilities of geometric and materials modeling have been obtained and illustrated. In the conventional level set methods, the governing Hamilton-Jacobi partial differential equation (PDE) was often solved by a finite difference method using the upwind schemes [Sethian (1999); Osher and Fedkiw (2001); Osher and Fedkiw (2002); Wang, Wang, and Guo (2003); Allaire, Jouve, and Toader (2004); Wang and Wang (2004b)], however, the time step size may be greatly constrained by a Courant-Friedrichs-Lewy (CFL) condition [Sethian (1999); Osher and Fedkiw (2002)] due to the explicit time integration schemes. To overcome this drawback, a semi-Lagrangian method was developed in [Xia, Wang, Wang, and Chen (2005)]. The level set Hamilton-Jacobi PDE was solved by an unconditionally stable semi-Lagrange scheme and it was reported that a much larger time step size could be used to save the computational time. More recently, Wang and Wang [Wang and Wang (2005d)] explored the use of RBFs for the level set-based structural topology optimization. The implicit level set function was defined by the multiquadric (MQ) RBF splines and the optimal front propagation can be obtained by solving a nonlinear coupled ODE. However, only some preliminary results were illustrated and the more challenging issues such as appropriate choice of RBF splines and initial designs, control of time step size in the time integration scheme, calculation of the Lagrange multiplier and determination of extension velocities were not fully addressed.

The distinct advantages of the level set methods based on embedding the interface as the zero-level set of a higher-dimensional function are well known. Generally, the level set methods provide a smooth geometrical description of the interface and require a relatively simple implementation and their extension to three-dimensional (3D) problems is straightforward [Peng, Merriman, Osher, Zhao, and Kang (1999); Gómez, Hernández, and López (2005)]. However, in applying a level set method for structural shape and topology optimization, the numerically complicated PDE solving procedures are usually necessary since the implementation of the conventional discrete level set methods requires appropriate choice of the upwind schemes, extension velocity methods and reinitialization algorithms, each of which may involve a PDE to be solved [Sethian (1999); Osher and Fedkiw (2001); Osher and Fedkiw (2002); Wang, Wang, and Guo (2003); Allaire, Jouve, and Toader (2004); Wang and Wang (2004b)]. In general, it is well known that the PDEs are rarely easy to implement [Mitchell (2004)], though some robust and accurate upwind schemes [Osher and Sethian (1988); Osher and Shu (1991); Jiang and Peng (2000)], fast marching methods [Sethian (1999)] and fast local level set methods [Peng, Merriman, Osher, Zhao, and Kang (1999); Gómez, Hernández, and López (2005)] have been presented in the literature. Furthermore, there is no nucleation mechanism to create new hole in the conventional level set methods, since the Hamilton-Jacobi equation is solved under a strict condition for numerical stability and reinitialization is applied to the level set function to ensure its regularity [Sethian (1999); Tsai and Osher (2003); Allaire, Gournay, Jouve, and Toader (2004); Burger, Hackl, and Ring (2004); Wang and Wang (2005d)]. Although some attempts have been made to incorporate both the topological derivatives and the shape derivatives into the level set methods to resolve this problem [Burger, Hackl, and Ring (2004); Allaire, Gournay, Jouve, and Toader (2004)], it is shown to be difficult to switch between the topological derivatives and the shape derivatives [Allaire, Gournay, Jouve, and Toader (2004); Wang, Mei, and Wang (2004)] and to handle surface functions [Burger (2004)]. Hence, the distinct advantages of the level set methods may be severely limited due to the numerical considerations of discrete computation for structural shape and topology optimization.

The objective of this study is to develop a more ef-

ficient implicit free boundary parametrization method as an effective level set-based alternative approach for both structural shape and topology optimization. Inverse multiquadric RBF splines are used to represent the implicit level set function with a high level of accuracy and smoothness. The original Hamilton-Jacobi PDE is converted into a mathematically more convenient ODE and the original time dependent initial value problem is changed to a time dependent interpolation problem for the initial values of the generalized expansion coefficients. In order to solve these coefficients, a collocation formulation of the method of lines is presented to generate a set of coupled non-linear ODEs, which can be readily solved by the existing ODE solvers. The periodic reinitialization process is eliminated to allow for the nucleation of new holes. The normal velocities at the free boundary are chosen to perform a steepest gradient-based shape and topology optimization. The normal velocity at the free boundary of the structure is finally determined by the strain energy density and a Lagrange multiplier. A bisectioning algorithm based on an implicit scheme is proposed to find the Lagrange multiplier to ensure that the optimal solution is always in the feasible domain. The extension velocities are obtained by extending the normal velocities at the free boundary to the whole design domain and a linear smoothing filter is used to smooth out the discontinuity at the free boundary. The present method is implemented in the framework of topological optimum of minimum compliance design that has been extensively studied in topology optimization and its efficiency and accuracy over the existing methods are highlighted. Numerical examples are chosen to illustrate the success of the present method in accuracy, convergence speed and insensitivity to initial designs in topology optimization of 2D problems.

2 Basic Formulation of the Conventional Level Set Methods

Level set methods first devised by Osher and Sethian (Osher and Sethian, 1988) have become popular recently for tracking, modeling and simulating the motion of dynamic interfaces (moving free boundaries) in fluid mechanics, combustion, computer animation, material science, crack propagation and image processing [Sethian (1999); Osher and Fedkiw (2002)]. These interfaces, which are usually the boundaries between different media, may develop sharp corners, break apart, merge to-

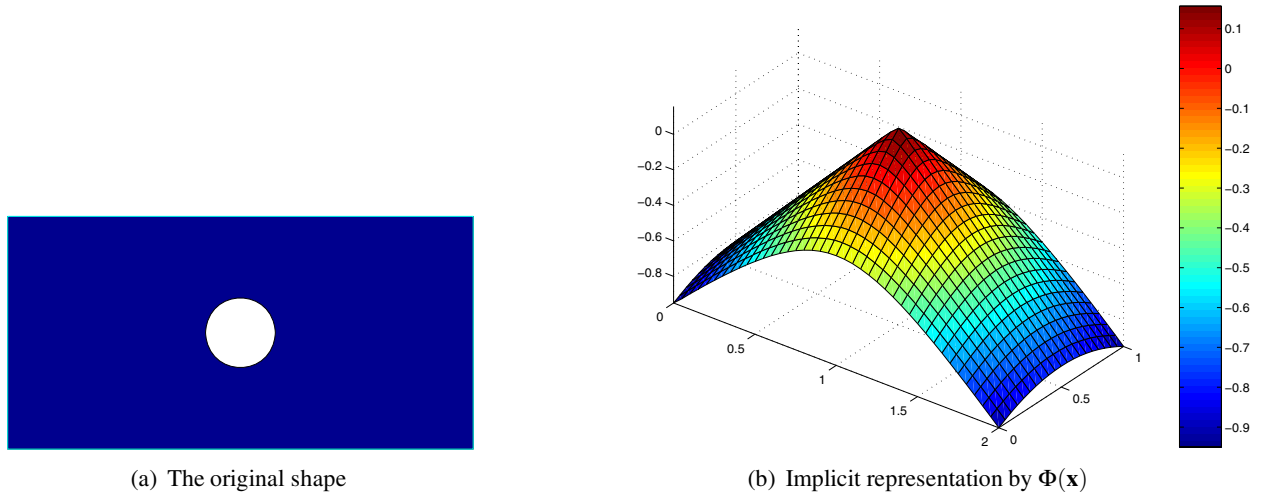


Figure 1 : Implicit representation of a 2×1 plate with a central hole.

gether or even disappear in an automatic way during the course of evolution, according to their own geometries or the laws of physics associated with the problem [Tsai and Osher (2003)]. Level set methods are developed to handle these topological changes by solving a particular class of PDEs—a hyperbolic PDE with first order time derivatives, also called a Hamilton-Jacobi PDE.

Usually, a level set method includes an implicit data representation of a dynamic interface, a set of Hamilton-Jacobi PDEs that govern the motion of the interface, and the corresponding implementations of numerical methods [Tsai and Osher (2003)]. The interface (front) that is represented is generally called hypersurface or surface. It is closed, nonintersecting and Lipschitz-continuous. The surface is represented implicitly through a Lipschitz-continuous level set function $\Phi(\mathbf{x})$, and the surface itself is the zero isosurface or zero level set $\{\mathbf{x} \in \mathbb{R}^d \mid \Phi(\mathbf{x}) = 0\}$ ($d = 2$ or 3). The embedding $\Phi(\mathbf{x})$ of $(d + 1)$ dimension can be specified in any specific form, for example, as a regular sampling on a rectilinear grid. Furthermore, $\Phi(\mathbf{x})$ can be used to define the inside and outside regions of the surface as follows:

$$\begin{aligned} \Phi(\mathbf{x}) &= 0 & \forall \mathbf{x} \in \partial\Omega \cap D \\ \Phi(\mathbf{x}) &< 0 & \forall \mathbf{x} \in \Omega \setminus \partial\Omega \\ \Phi(\mathbf{x}) &> 0 & \forall \mathbf{x} \in (D \setminus \Omega) \end{aligned} \quad (1)$$

where $D \subset \mathbb{R}^d$ is a fixed design domain in which all admissible shapes Ω (a smooth bounded open set) are included, i.e. $\Omega \subset D$. Figure 1 illustrates this implicit rep-

resentation of the shape of a 2×1 plate with a central hole, in which the boundary of the central hole is represented by $\Phi(\mathbf{x}) = 0$. The local unit normal to the surface n can be given by

$$n = \frac{\nabla\Phi}{|\nabla\Phi|}, \quad |\nabla\Phi| = \sqrt{\nabla\Phi \cdot \nabla\Phi} \quad (2)$$

In the level set methods, it is convenient to use the Heaviside step function H and the Dirac delta function δ defined [Wang, Wang, and Guo (2003); Burger (2004)] as

$$H(\Phi) = \begin{cases} 1, & \Phi \geq 0 \\ 0, & \Phi < 0 \end{cases}, \quad \delta(\Phi) = H'(\Phi) \quad (3)$$

Then, the interior and the boundary Γ of a shape can be described in terms of the level set function $\Phi(\mathbf{x})$ respectively as

$$\Omega = \{\mathbf{x} : H(-\Phi(\mathbf{x})) = 1\}, \quad \Gamma = \{\mathbf{x} : \delta(\Phi(\mathbf{x})) > 0\} \quad (4)$$

Furthermore, in the level set formulation, the volume integral of a function $F(\mathbf{x})$ is defined as

$$\int_D F(\mathbf{x}) H(-\Phi) d\Omega$$

If $F(\mathbf{x}) \equiv 1$, this integral yields the volume $V(\Phi)$ as follows:

$$V(\Phi) = \int_D H(-\Phi) d\Omega \quad (5)$$

To let the level set function dynamically change in time, a continuous velocity field v , which is a function of position \mathbf{x} and some other geometrical or physical quantities, is introduced and the evolution can be described as the following Cauchy problem [Tsai and Osher (2003)]:

$$\frac{\partial \Phi}{\partial t} + v \cdot \nabla \Phi = 0, \quad \Phi(\mathbf{x}, 0) = \Phi_0(\mathbf{x}) \quad (6)$$

where $\Phi_0(\mathbf{x})$ embeds the initial position of the surface and t the artificial time. According to Eq. (2), Eq. (6) can be re-written using the normal velocity v_n as

$$\frac{\partial \Phi}{\partial t} + v_n |\nabla \Phi| = 0, \quad \Phi(\mathbf{x}, 0) = \Phi_0(\mathbf{x}) \quad (7)$$

where

$$v_n = v \cdot \frac{\nabla \Phi}{|\nabla \Phi|} \quad (8)$$

It should be noted that Eqs. (6) and (7) are the usually fully non-linear first order Hamilton-Jacobi or second order degenerate parabolic equations, and with suitable restrictions, the theory of viscosity solutions can be applied to guarantee the well-posedness of the Cauchy problem [Crandall and Lions (1984); Sethian (1999); Osher and Fedkiw (2002); Tsai and Osher (2003)]. To time advance the solutions, a common numerical practice is to use a fixed grid to capture the surface. In this Eulerian type approach the normal velocity v_n defined at the surface or front must be extended to the grid points either in the whole design domain D [Allaire, Jouve, and Toader (2004)] or a narrow band [Osher and Fedkiw (2002)]. The extension velocities are often obtained by a PDE solving procedure such as the fast marching methods [Sethian (1999)] in the conventional level set methods. The choice of extension velocities can directly influence the overall efficiency [Richards, Bloomfield, Sen, and Calea (2001)].

In many situations, the level set function will develop steep and/or flat gradients leading to problems in numerical approximations [Peng, Merriman, Osher, Zhao, and Kang (1999); Tsai and Osher (2003)]. It is thus needed to reinitialize the level set function to resurrect the behavior of $\Phi(\mathbf{x})$ in the neighborhood of the front, while keeping the zero location unchanged. Reinitialization is usually applied as an auxiliary step, but it can be very important to guarantee a good approximation of the normal or the curvature of the free boundary. For most applications, it is important to use a high order discretization

method in the reinitialization algorithms [Tsai and Osher (2003)] since the location of the original interface may be perturbed apparently by the numerical diffusion. Furthermore, global reinitialization in the computational domain will prevent new holes from appearing. Thus, special treatment must be taken if emergence of new holes is of interest [Tsai and Osher (2003); Burger, Hackl, and Ring (2004)].

Since a general analytical solution to the implicit function $\Phi(\mathbf{x}, t)$ in the non-linear first order Hamilton-Jacobi PDE (7) is usually unavailable, a numerical procedure for solving the Hamilton-Jacobi PDE (7) is indispensable. This procedure requires appropriate choice of the complicated PDE solving upwind schemes, reinitialization algorithms and extension velocity methods, which may limit the utility of the level set methods as aforementioned. Some of the limitations may become totally undesirable in structural shape and topology optimization. As above-mentioned, global reinitialization prevents a level set function from creating new holes in the interior of material regions [Sethian (1999); Tsai and Osher (2003); Burger, Hackl, and Ring (2004)], which will make the final optimum severely dependent of the initial design [Allaire, Jouve, and Toader (2004)]. Another major limitation lies in the discrete representation due to the Eulerian approach used in the conventional level set methods [Sethian and Wiegmann (2000); Osher and Fedkiw (2002); Allaire, Jouve, and Toader (2004); Wang, Wang, and Guo (2003)]. Since the grid of the finite difference method in the Eulerian approach is fixed in space, the geometry (or topology) can only be described by the nodal values of $\Phi(\mathbf{x})$ and shape functions to ensure that the space of achievable designs will be smooth enough in shape [Belytschko, Xiao, and Parimi (2003); Wang, Wang, and Guo (2003)]. Usually, only the implicit function $\Phi(\mathbf{x})$, rather than its partial derivatives, can be guaranteed to be continuous across the meshes because of the notorious polynomial snaking problem that polynomial interpolation in high dimensions can easily lead to singular problems and cause derivative estimates to be very poor [Kansa (1990); Kansa, Powerb, Fasshauer, and Ling (2004)]. The mesh spacing must be sufficiently fine to capture the spatial partial derivative behavior accurately and to avoid numerical artifacts contaminating the solution. This makes the computation quite time and memory consuming. Furthermore, the widely adopted explicit time derivative approximation schemes are sub-

ject to the time step restrictions dictated by the CFL condition to guarantee a stable convergence [Osher and Fedkiw (2002)]. In case that a sufficiently fine mesh is adopted, time step sizes may be not chosen to satisfy the accuracy requirements but rather to satisfy the CFL condition, which will make the time step sizes overly small and the computational cost unnecessarily too expansive [Enright, Losasso, and Fedkiw (2005)].

Therefore, a better method is to preserve the topological benefits of implicit representation of a level set method while avoiding the drawbacks of using its discrete samples on a fixed grid. To this end, the level set method using the implicit RBF modeling first proposed for topology optimization by the authors [Wang and Wang (2005d)] is further developed for simultaneous shape and topology optimization of structures. The implicit level set function $\Phi(t, \mathbf{x})$ is to be replaced by an implicit free boundary representation method which provides a free-form representation with parameterization. The detailed discussion is to be given in the following sections.

3 An Implicit Free Boundary Parameterization Method

The implicit free boundary in the level set methods is parameterized by the inverse multiquadric RBF splines. Global smoothness of the implicit function can be obtained and the accuracy and efficiency of a level set model is thus improved. The original time-dependent initial value problem is converted into a mathematically more convenient time-dependent interpolation problem for the initial values of the generalized expansion coefficients of the RBF interpolant. The motion of the free boundary is governed by a time dependent coupled non-linear ODE and the eigenvalue stability of the inverse multiquadric RBFs can guarantee a CFL-free time advancement of the free boundary. Moreover, reinitialization becomes unnecessary and is thus eliminated to allow for the nucleation of new holes inside the material domain to generate initial design-insensitive optimal solutions.

3.1 RBF Parameterization Method for the Implicit Free Boundary

To model and reconstruct the entire admissible design with an implicit level set function which is globally

continuous and differentiable, an implicit free boundary parameterization method is presented using the RBFs, which are popular for interpolating scattered data to produce smooth surface/boundary as the associated system of non-linear equations is guaranteed to be invertible under mild conditions on the locations of the data points [Carr, Beatson, Cherrie, Mitchell, Fright, McCallum, and Evans (2001)]. Radial basis functions have gained considerable success for decades as basis functions for interpolating scattered data in higher-dimensional spaces [Cheng, Golberg, Kansa, and Zammito (2003)]. Their theoretical basis and convergence properties were intensively investigated and a thorough theoretical and implementation viewpoints on RBFs can be found in [Buhmann (2004)]. In real-world applications, radial basis functions have become extremely useful, ranging from pattern reconstruction, artificial intelligence [Buhmann (2004)], to simply solving mathematical PDEs [Cheng, Golberg, Kansa, and Zammito (2003); Cecil, Qian, and Osher (2004)]. The positive features of RBFs such as the unique solvability of the interpolation problem and their excellent smoothness and convergence make them very attractive in the level set methods [Wang and Wang (2005d)]. In the present study, the RBF implicit modeling is to be presented as an effective parameterization method to reconstruct the moving free boundary in the level set methods.

Radial basis functions are radially-symmetric functions centered at a particular point [Morse, Yoo, Chen, Rheingans, and Subramanian (2001)], or knot, which can be expressed as follows:

$$\varphi_i(\mathbf{x}) = \varphi(\|\mathbf{x} - \mathbf{x}_i\|), \quad \mathbf{x}_i \in D \quad (9)$$

where $\|\cdot\|$ denotes the Euclidean norm on \mathbb{R}^d [Cheng, Golberg, Kansa, and Zammito (2003)], and \mathbf{x}_i the position of the knot. Only a single fixed function form $\varphi: \mathbb{R}^+ \rightarrow \mathbb{R}$ with $\varphi(0) \geq 0$ is used as the basis to form a family of independent functions. There is a large class of possible radial basis functions. Commonly used RBFs include thin-plate spline, polyharmonic splines, Sobolev splines, Gaussians, multiquadrics, inverse multiquadrics and compactly supported RBFs [Cheng, Golberg, Kansa, and Zammito (2003); Kansa, Powerb, Fasshauer, and Ling (2004)]. Among these common functions, the multiquadric (MQ) spline suggested by Hardy [Hardy (1990)] has been well accepted by some researchers

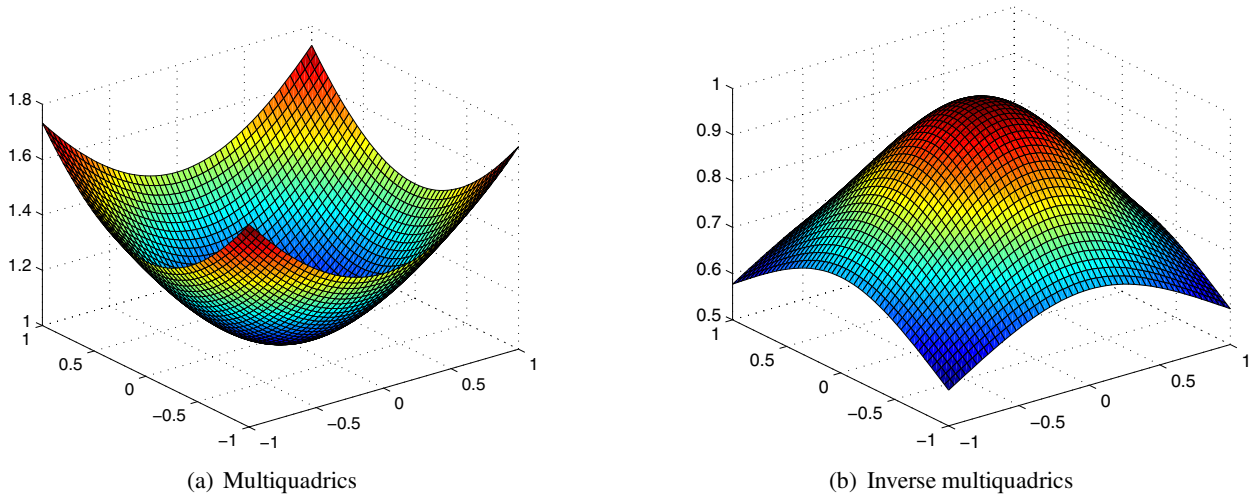


Figure 2 : Two infinitely smooth RBF splines with a free shape parameter of $c = 1$.

[Franke (1982); Cheng, Golberg, Kansa, and Zammito (2003); Kansa, Powerb, Fasshauerc, and Ling (2004); Wang and Wang (2005d)], which can be written as

$$\varphi_i(\mathbf{x}) = \sqrt{(\mathbf{x} - \mathbf{x}_i)^2 + c_i^2} \quad (10)$$

where c_i is the free shape parameter which is commonly assumed to be a constant for all i in most applications [Cheng, Golberg, Kansa, and Zammito (2003)]. This RBF spline was ranked the best in interpolation for scattered data by Franke [Franke (1982)]. However, the MQ is only conditionally positive definite [Cheng, Golberg, Kansa, and Zammito (2003)] and has to be augmented by a leading constant term in the series and higher-order MQs require more terms in the polynomial [Schaback and Wendland (2001)]. On the other hand, the inverse multiquadric (IMQ), which can be expressed as

$$\varphi_i(\mathbf{x}) = \frac{1}{\sqrt{(\mathbf{x} - \mathbf{x}_i)^2 + c_i^2}} \quad (11)$$

is positive definite [Cheng, Golberg, Kansa, and Zammito (2003)] and can be used without augmentation. Figure 2 displays a multiquadric spline and an inverse multiquadric spline with a free shape parameter of $c = 1$. Since a free shape parameter is included in these splines, they are all infinitely smooth, different from those parameter-free splines such as cubic splines and thin plate splines, which are piecewise smooth only (Platte and Driscoll, 2005).

In the present study, for the purpose of numerical convenience, the IMQ shown in Eq. (11), rather than the more widely used MQ shown in Eq. (10), is used to interpolate the scalar implicit level set function $\Phi(\mathbf{x})$ with N knots by using N IMQs centered at these knots. The resulting RBF interpolant of the implicit function can be written as

$$\Phi(\mathbf{x}) = \sum_{i=1}^N \alpha_i \varphi_i(\mathbf{x}) \quad (12)$$

where α_i is the weight, or expansion coefficient, of the IMQ positioned at the i -th knot. Hence, the implicit level set function is parameterized by the infinitely smooth IMQ radial basis functions. Since the free boundary is embedded in the implicit level set function as the zero level set, it is thus parameterized implicitly. It should be noted that different from the work in [Wang and Wang (2005d)] using the MQs, the augmentation terms are not included in the present study due to the use of IMQs. Furthermore, according to [Cheng, Golberg, Kansa, and Zammito (2003)], using the inverse multiquadrics as the basis function, an appealing exponential convergence rate $O(\lambda^{\sqrt{c}/h})$, where h is the mesh size and $0 < \lambda < 1$, in the numerical solutions can be obtained. Therefore, the present parameterization method using the IMQ RBFs can achieve a high level of accuracy and smoothness of the implicit level set function. If the interpolation data values $f_1, \dots, f_N \in \mathbb{R}$ at knot locations $\mathbf{x}_1, \dots, \mathbf{x}_N \in D \subset \mathbb{R}^d$ are given, the RBF interpolant of $\Phi(\mathbf{x})$ in Eq. (12) can be obtained by solving the system of N linear equa-

tions for N unknown generalized expansion coefficients as follows:

$$\Phi(\mathbf{x}_i) = f_i, \quad i = 1, \dots, N \quad (13)$$

which can be given in matrix form as

$$\mathbf{H}\boldsymbol{\alpha} = \mathbf{f} \quad (14)$$

where

$$\mathbf{H} = \begin{bmatrix} \varphi_1(\mathbf{x}_1) & \cdots & \varphi_N(\mathbf{x}_1) \\ \vdots & \ddots & \vdots \\ \varphi_1(\mathbf{x}_N) & \cdots & \varphi_N(\mathbf{x}_N) \end{bmatrix} \in \mathbb{R}^{N \times N} \quad (15)$$

$$\boldsymbol{\alpha} = [\alpha_1 \quad \cdots \quad \alpha_N]^T \in \mathbb{R}^N \quad (16)$$

$$\mathbf{f} = [f_1 \quad \cdots \quad f_N]^T \in \mathbb{R}^N \quad (17)$$

Since the IMQ collocation matrix \mathbf{H} is theoretically invertible due to the positive definiteness of the IMQs [Buhmann (2004); Kansa, Powerb, Fasshauerc, and Ling (2004)], the generalized expansion coefficients $\boldsymbol{\alpha}$ can be simply given by

$$\boldsymbol{\alpha} = \mathbf{H}^{-1}\mathbf{f} \quad (18)$$

After obtaining the generalized expansion coefficients $\boldsymbol{\alpha}$, the resulting RBF interpolant of the implicit function in Eq. (12) can be re-written compactly as

$$\Phi(\mathbf{x}) = \boldsymbol{\phi}^T(\mathbf{x})\boldsymbol{\alpha} \quad (19)$$

where

$$\boldsymbol{\phi}(\mathbf{x}) = [\varphi_1(\mathbf{x}) \quad \cdots \quad \varphi_N(\mathbf{x})]^T \in \mathbb{R}^N \quad (20)$$

However, with the increase of the matrix dimension, the time required to compute the inverse of \mathbf{H} may become unacceptable because the IMQ collocation matrix \mathbf{H} is a symmetric full matrix only. To solve Eq. (14) for relatively simple and small-size problems effectively, it is possible to use the LU factorization (an $O((N+4)^3)$ algorithm) or iterative means in $O((N+4)^2)$ [Morse, Yoo, Chen, Rheingans, and Subramanian (2001)]. Nevertheless, these methods may become computationally too expensive and even impractical [Carr, Beatson, Cherrie, Mitchell, Fright, McCallum, and Evans (2001)] when applied to large-scale and/or 3D problems. Hence, the fast evaluation methods [Carr, Beatson, Cherrie, Mitchell, Fright, McCallum, and Evans (2001)] based on the

Fast Multipole Method (FMM) [Greengard and Rokhlin (1987)], which can greatly reduce the storage and computational cost of using RBFs, should be adopted. It should also be noted that the distribution of the RBF sampling knots in RBF implicit modeling is relatively free. Hence, different from the conventional level set method using a fixed regular uniform grid only, both uniform and non-uniform grids can be used in the present RBF implicit modeling. This may become a definite advantage when a non-uniform or unstructured mesh becomes necessary for the accurate and efficient analysis of the physics associated with the problem.

3.2 Governing Equation of Motion of the Implicit Free Boundary

The presented RBF implicit modeling for the level set function $\Phi(\mathbf{x})$ is used to transform the Hamilton-Jacobi time dependent PDE into a system of time dependent ordinary differential equations (ODEs) over the entire domain D to achieve a significant mathematical convenience. As aforementioned, in the conventional level set methods, moving the free boundary is equivalent to transporting the scalar implicit function $\Phi(\mathbf{x})$ by solving the Hamilton-Jacobi PDE (7) and thus the motion of the free boundary (zero level sets) is governed by the Hamilton-Jacobi PDE. Since the Hamilton-Jacobi PDE (7) is time dependent, in the present RBF implicit modeling for the level set function $\Phi(\mathbf{x})$, it is further assumed that all the knots are fixed in space and the space and time are separable and the time dependence of the implicit function Φ is due to the generalized expansion coefficients $\boldsymbol{\alpha}$ of the RBF interpolant in Eq. (16). With these assumptions, the RBF interpolant of the implicit function in Eq. (19) becomes time dependent as

$$\Phi = \Phi(\mathbf{x}, t) = \boldsymbol{\phi}^T(\mathbf{x})\boldsymbol{\alpha}(t) \quad (21)$$

Substituting Eq. (21) into the Hamilton-Jacobi PDE defined in (7) yields

$$\boldsymbol{\phi}^T \frac{d\boldsymbol{\alpha}}{dt} + v_n |(\nabla\boldsymbol{\phi})^T \boldsymbol{\alpha}| = 0 \quad (22)$$

where

$$|(\nabla\boldsymbol{\phi})^T \boldsymbol{\alpha}| = \left[\left(\frac{\partial\boldsymbol{\phi}^T}{\partial x} \boldsymbol{\alpha} \right)^2 + \left(\frac{\partial\boldsymbol{\phi}^T}{\partial y} \boldsymbol{\alpha} \right)^2 + \left(\frac{\partial\boldsymbol{\phi}^T}{\partial z} \boldsymbol{\alpha} \right)^2 \right]^{1/2} \quad (23)$$

In Eq. (22), the RBF expansion coefficients are explicitly time dependent and all the time dependence is due to the expansion coefficients. At the initial time, all the time dependent variables should be specified over the entire domain. This initial value problem can be considered equivalent to an interpolation problem since the expansion coefficients at the initial time are found as a solution of the interpolation problem, as shown in Eq. (14). Hence, the preliminary starting point of the use of RBFs to solve PDEs is the interpolation problem that is equivalent to solving the initial value problem. The original time-dependent initial value problem defined by the Hamilton-Jacobi PDE (7) in the conventional level set methods is thus converted into a time-dependent interpolation problem for the initial values of the generalized expansion coefficients $\boldsymbol{\alpha}$ and the motion of the free boundary, or the propagation of the front, is now governed by the time dependent coupled ODE (22).

To time advance the initial values $\boldsymbol{\alpha}$ in the governing equation of motion (22), a collocation formulation of the method of lines is presented because of its inherent simplicity. The governing equation of motion of the implicit free boundary Eq. (22) is extended to the whole design domain D and the normal velocities v_n at the implicit free boundary are thus replaced by the extension velocities v_n^e in D . Based on the principle of collocation method, all nodes of the spatial discretization of the extended ODE (22) are located sequentially at the fixed knots of the RBF interpolation for the implicit function $\Phi(\mathbf{x})$. Furthermore, in the present implementation, for the purpose of simplicity, all the nodes of a fixed mesh for structural analysis are taken as the fixed knots of RBF interpolation, though not necessary. By using this collocation method, a set of ODEs can be compactly written as follows:

$$\mathbf{H} \frac{d\boldsymbol{\alpha}}{dt} + \mathbf{B}(\boldsymbol{\alpha}) = 0 \quad (24)$$

where

$$\mathbf{B}(\boldsymbol{\alpha}) = [v_n^e(\mathbf{x}_1) | (\nabla\Phi^T(\mathbf{x}_1))\boldsymbol{\alpha}| \ \cdots \ v_n^e(\mathbf{x}_N) | (\nabla\Phi^T(\mathbf{x}_N))\boldsymbol{\alpha}]^T \quad (25)$$

It should be noted that Eq. (24) can be regarded as a collocation formulation of the general method of lines [Madsen (1975)], in which a time dependent PDE problem is reduced to a simpler time dependent ODE problem by discretization, though only a time dependent coupled ODE is involved in the present problem and thus using

finite difference relationships for the spatial derivatives is not needed. The method of lines has a solid mathematical foundation and the convergence of the solution of the converted ODE problem to the solution of the original PDE problem has been rigorously proven [Madsen (1975)].

The set of coupled non-linear ODEs of Eq. (24) can be solved by several well-established ODE solvers such as the first-order forward Euler's method and higher-order Runge-Kutta, Runge-Kutta-Fehlberg, Adams-Bashforth, or Adams-Moulton methods [Greenberg (1998)]. In the present study, only the first-order forward Euler's method is used since it is the simplest solution algorithm for ODE initial condition problems and often used for comparison with more accurate algorithms, which are more complex and tedious to implement. Using Euler's method, an approximate solution to Eq. (24) can be given by

$$\boldsymbol{\alpha}(t^{n+1}) = \boldsymbol{\alpha}(t^n) - \tau \mathbf{H}^{-1} \mathbf{B}(\boldsymbol{\alpha}(t^n)) \quad (26)$$

where τ is the step size. Because of the fixed location of the RBF knots, the IMQ collocation matrix \mathbf{H} is time independent. Hence, only storing the initial value of its inverse matrix will greatly save the computational time. In the conventional level set methods, the time step size should be sufficiently small to achieve the numerical stability due to the CFL condition that the CFL number must be less than or equal to one for stability in the von Neumann sense [Osher and Fedkiw (2002)] and to reduce the truncation error due to the spatial discretization. In the present method, since the IMQs are positive definite RBFs [Schaback and Wendland (2001)] and boundary-condition free (radially unbounded), according to a recent result in [Platte and Driscoll (2005)], the present implementation of the method of lines is time-stable for all knot distributions and thus CFL-free. Hence, the timestep constraint resulting from the CFL condition can be significantly relaxed, which may become quite attractive in high-speed and fine-grid calculations.

Because of the necessary use of upwind differencing at each step, the conventional level set methods have a tendency to lose surface in under-resolved regions [Lageste and Pitsch (2002)] or unwanted dissipation of the front [Sussman and Fatemi (1999)]. A reinitialization procedure is thus needed to resurrect the behavior of the level set function $\Phi(\mathbf{x})$ in the neighborhood of the front to guarantee a good approximation of the normal or the curvature of the front. However, reinitialization error is

likely to accumulate as the number of time steps grows. The quite common iterative reinitialization scheme based on a signed distance function has a potential disadvantage in the relative crudeness of the switch function based on checking the sign of the level set equation, which may cause the front to move [Sethian (1999)]. In the existing level set-based topology optimization methods in the literature [Allaire, Jouve, and Toader (2004); Wang, Wang, and Guo (2003)], reinitialization produces a severe problem that new holes cannot be created within a material region [Burger, Hackl, and Ring (2004); Allaire, Gournay, Jouve, and Toader (2004)]. Furthermore, the reinitialization procedure is usually time-consuming [Ye, Bresler, and Moulin (2002)]. Hence, reinitialization should be avoided as much as possible. In practice, whether reinitialization is appropriate should depend on whether the underlying problem is interested in only the zero level set of function, or the entire level set function $\Phi(\mathbf{x})$.

In the present level set method, moving the free boundary is equivalent to transporting the scalar implicit function $\Phi(\mathbf{x})$ by solving the system of coupled non-linear time dependent ODEs of Eq. (24). The upwind difference methods [Osher and Sethian (1988); Jiang and Peng (2000); Osher and Shu (1991)] popular in the conventional level set methods are not employed to advance the front in the present study since spatial derivatives of the level set function can be obtained analytically and a good behavior of the normal or curvature of the front can be maintained due to the infinite and global smoothness of the IMQ splines [Cheng, Golberg, Kansa, and Zammito (2003)]. Therefore, reinitialization is not performed in the present level set application for classical shape and topology optimization and the entire level set function $\Phi(\mathbf{x})$ is taken into account. Thus, the present level set model is capable of hole nucleation and elimination of the dependency of the final optimal solution on the design initiation in shape and topology optimization. As suggested by Sethian [Sethian (1999)], possible problems with loss of mass or movement of the zero level set without reinitialization can be avoided if an appropriate extension velocity method is adopted. In the present study, a straightforward and efficient mass conservative extension velocity method is proposed for both structural shape and topology optimization, which will be discussed in detail as follows.

4 Simultaneous Shape and Topology Optimization Using the Level Set Method

The proposed shape and topology optimization process operates on the implicit scalar level set function $\Phi(\mathbf{x})$ defined in Eq. (1) and represented by the IMQ RBF implicit modeling in (19) and uses a steepest gradient method to find the decent direction of the normal velocity for the minimization of an objective function $J(\Phi)$. The normal velocity at the implicit free boundary is naturally and smoothly extended to the whole design domain D without using any additional PDE solving procedure to keep the mass conservative during the evolution.

4.1 Minimum Compliance Design

In the classical shape and topology optimization problems, the minimum compliance design has been widely investigated. With a level set model as shown in Eq. (1), the standard notion [Bendsøe and Sigmund (2003)] of a classical minimum compliance design problem can be rewritten as follows:

$$\begin{aligned} \text{Minimize}_{\Phi} \quad & J(\mathbf{u}, \Phi) = \int_D (\boldsymbol{\varepsilon}(\mathbf{u}))^T \mathbf{C} \boldsymbol{\varepsilon}(\mathbf{u}) H(-\Phi) d\Omega \\ \text{subject to:} \quad & a(\mathbf{u}, \mathbf{v}, \Phi) = L(\mathbf{v}, \Phi), \quad \mathbf{u}|_{\Gamma_D} = \mathbf{u}_0, \quad \forall \mathbf{v} \in U \\ & V(\Phi)/V_0 = \zeta \end{aligned} \quad (27)$$

where $J(\mathbf{u}, \Phi)$ is the objective function, \mathbf{u} the displacement field, $\boldsymbol{\varepsilon}(\mathbf{u})$ the strain field, \mathbf{C} the Hook elasticity tensor, $V(\Phi)$ the material volume as defined in Eq. (5), V_0 the design domain volume and ζ the prescribed volume fraction. The linear elastic equilibrium equation is written in its weak variational form in terms of the energy bilinear form $a(\mathbf{u}, \mathbf{v}, \Phi)$ and the load linear form $L(\mathbf{v}, \Phi)$ [Bendsøe and Sigmund (2003)], with \mathbf{v} denoting a virtual displacement field in the space U of kinematically admissible displacement fields, and \mathbf{u}_0 the prescribed displacement on the admissible Dirichlet boundary Γ_D .

The Lagrange multiplier method [Osher and Santosa (2001)] can be used to solve the present optimization problem (27) of minimum compliance design. By setting the constraint on the equilibrium state inactive, the Lagrangian $\mathcal{L}(\mathbf{u}, \Phi, \ell)$ with a positive Lagrange multiplier ℓ can be given by

$$\mathcal{L}(\mathbf{u}, \Phi, \ell) = J(\mathbf{u}, \Phi) + \ell G(\Phi) \quad (28)$$

where the constraint function $G(\Phi)$ can be expressed as

$$G(\Phi) = V(\Phi) - \zeta V_0 = 0 \quad (29)$$

It should be noted that the displacement field \mathbf{u} is also a function of Φ , i.e. $\mathbf{u} = \mathbf{u}(\Phi)$ since the mechanical response will change with the geometry. According to the Kuhn-Tucker condition of the optimization [Osher and Santosa (2001)], the necessary condition for a minimizer is

$$D_{\Phi} \mathcal{L}(\mathbf{u}(\Phi), \Phi, \ell) = 0 \quad (30)$$

where $D_{\Phi} \mathcal{L}(\mathbf{u}(\Phi), \Phi, \ell)$ is the gradient of the Lagrangian with respect to Φ . Hence, both Φ and ℓ can be found by solving Eqs. (29) and (30).

4.2 Shape Derivatives

The gradient of the Lagrangian $D_{\Phi} \mathcal{L}(\mathbf{u}(\Phi), \Phi, \ell)$ may be obtained in a number of different ways following the well-known approach of Murat and Simon of shape diffeomorphism [Sokolowski and Zolesio (1992)]. In the present study, the shape sensitivity analysis presented by Allaire et al. [Allaire, Jouve, and Toader (2004)] is adopted to derive the shape derivatives.

Usually, the boundary ∂D of the whole structural shape and topology design domain D can be decomposed [Allaire, Jouve, and Toader (2004)] as

$$\partial D = \partial D_D \cup \partial D_N \cup \partial D_H \quad (31)$$

where ∂D_D is the Dirichlet boundary, ∂D_N the non-homogeneous Neumann boundary, and ∂D_H the homogeneous Neumann boundary (traction free). To derive the shape derivatives from the classical shape sensitivity analysis [Sokolowski and Zolesio (1992)], it is assumed that the shape boundary $\partial \Omega$ of an admissible design Ω can satisfy the following conditions:

$$\partial \Omega = \Gamma_D \cup \Gamma_N, \quad \Gamma_D \subset \partial D_D, \quad \Gamma_N = \partial D_N \cup \Gamma_H \quad (32)$$

where Γ_D is the admissible Dirichlet boundary, Γ_N the Neumann boundary, and Γ_H the homogeneous Neumann boundary. Furthermore, it is assumed that the surface loads are design independent and applied only on a fixed subset of the boundary Γ_N and the Dirichlet boundary Γ_D is with zero displacements. The whole traction free homogeneous Neumann boundary Γ_H may be represented by the zero level set function. However, in the initial

designs the strain energy density can be too high at the traction free boundary near the loading points at the non-homogeneous Neumann boundary or near the Dirichlet boundary due to the stress concentration, which may generate an undesirable maximum normal velocity in the early evolution as later discussed. Therefore, in the present shape and topology optimization, only part of the traction free homogeneous Neumann boundary $\Gamma_M \subset \Gamma_H$ is initially chosen to be optimized as the moving free boundary, which is represented by the dynamic interface $\Phi(\mathbf{x}) = 0$ in the present level set model. It should also be noted that this handling will not prevent the whole boundary from being optimized due to the optimal time propagation of the moving free boundary.

Based on local perturbations of the moving free boundary of an admissible design Ω [Allaire, Jouve, and Toader (2004)] (continuous perturbations with respect to the Hausdorff distance [Burger, Hackl, and Ring (2004)]), the resulting shape derivative of the Lagrangian can be written as

$$\frac{d\mathcal{L}}{dt} = \int_D (\ell - \boldsymbol{\varepsilon}^T \mathbf{C} \boldsymbol{\varepsilon}) \delta(\Phi) |\nabla \Phi| v_n d\Omega \quad (33)$$

which can be further simplified [Burger (2004)] as

$$\frac{d\mathcal{L}}{dt} = \int_{\Gamma_M} (\ell - \boldsymbol{\varepsilon}^T \mathbf{C} \boldsymbol{\varepsilon}) v_n ds \quad (34)$$

where t is the artificial time, and v_n the artificial normal velocity at the moving free boundary Γ_M . Furthermore, the resulting shape derivative of the volume constraint function $G(\Phi)$ (29) can be expressed as

$$\frac{dG}{dt} = \int_{\Gamma_M} v_n ds \quad (35)$$

Hence, these shape derivatives can be obtained from a surface integration. In a level set model, only the normal velocity field v_n , rather than these shape derivatives, is needed and thus it is unnecessary to perform an explicit surface integration. In the present shape and topology optimization, choosing the normal velocity field v_n is equivalent to choosing a descent direction for the objective function, which can be easily implemented by using a steepest gradient method [Osher and Santosa (2001); Wang, Wang, and Guo (2003); Allaire, Jouve, and Toader (2004)].

4.3 Normal Velocity Function

According to the shape derivative in Eq. (34), a descent direction of the normal velocity v_n for the Lagrangian can

be obtained by simply identifying the normal velocity v_n as

$$v_n = \boldsymbol{\varepsilon}^T \mathbf{C} \boldsymbol{\varepsilon} - \ell \quad (36)$$

in which the normal velocity v_n at the moving free boundary Γ_M can be determined by the strain energy density and a Lagrange multiplier. Hence, the normal velocity field is linked with the objective function of the present minimum compliance design problem and physics of the present problem is incorporated due to the flexibility of a level set model in choosing the velocity function. Without remeshing, the strain energy density field can be accurately and efficiently obtained numerically by using the “ersatz material” approach [Allaire, Jouve, and Toader (2004)], the geometry projection method [Norato, Haber, Tortorelli, and Bendsøe (2004)], the true meshless local Petrov-Galerkin method [Atluri and Shen (2002)], or some extended finite element methods [Belytschko and Black (1999); Strouboulis, Copps, and Babuska (2001); Wang and Wang (2005c)], though the standard finite element method without remeshing is not applicable due to the movement of the free boundary across the elements. However, the calculation of the Lagrange multiplier ℓ is not so straightforward.

To find the variable Lagrange multiplier ℓ , only several methods are available in the open literature, which appear to be less effective. In the work of [Allaire, Jouve, and Toader (2004)], as well as of [Wang and Wang (2005d)], a fixed ℓ was used during the evolution of the free boundary and thus the volume constraint cannot be satisfied and only an unconstrained optimization can be performed. The possible applications may become quite limited since the real-world optimization problems are usually constrained. In the work of [Wang, Wang, and Guo (2003)], the variable Lagrange multiplier was derived from an assumption that the material volume keeps constant during the evolution such that its shape derivative defined in (35) vanishes. However, this handling may become even conceptually problematic since the conventional level set methods cannot conserve the mass in the sense that no mass is lost or gained [Sethian (1999); Osher and Fedkiw (2002)] and thus the material volume will not be constant during the evolution. In fact, significant fluctuations of the material volume can be observed in their numerical results [Wang, Wang, and Guo (2003)]. In the work of Osher and Santosa [Osher and Santosa (2001)], the Lagrange multiplier was obtained based on

a similar assumption that the total material volume can be conserved, but the possible drift of the volume during the iteration was noticed and a Newton’s method was used to put the iteration back to the feasible set. In the work of Wang and Wang [Wang and Wang (2005c)], the material volume was also assumed to be conservative to find the Lagrange multiplier, but a higher or lower multiplier was used to push the volume back to satisfy the volume constraint during the evolution. All these methods cannot guarantee that the volume constraint function converge and thus the final solutions may become even infeasible.

Hence, a better way to calculate the Lagrange multiplier is that the Lagrange multiplier is chosen to make the volume constraint exactly satisfied at each iteration. In the present study, based on such a methodology, a bi-sectioning algorithm is proposed to find the Lagrange multiplier ℓ to guarantee that the volume constraint be exactly satisfied during the iteration.

4.4 Bi-sectioning Algorithm

A bi-sectioning algorithm is developed to determine the value of the Lagrange multiplier ℓ to satisfy the volume constraint at each time step based on the fact that the volume constraint function $G(\Phi)$ in (29) is a monotonously decreasing function of the Lagrange multiplier ℓ . By using the normal velocities defined in (36), the shape derivative of the volume constraint function $G(\Phi)$ in Eq. (35) can be re-written as

$$\frac{dG}{dt} = \int_{\Gamma_M} (\boldsymbol{\varepsilon}^T \mathbf{C} \boldsymbol{\varepsilon} - \ell) ds \quad (37)$$

from which it can be easily obtained that the $G(\Phi)$ decreases with a large value of ℓ and increases with a low value of ℓ . Hence, the bi-sectioning algorithm can be initialized by setting a lower ℓ_1 and an upper ℓ_2 bound for the Lagrange multiplier. In the present numerical study, it is initially chosen that $\ell_1 = 0$, which will cause a maximum volume increase, and $\ell_2 = 10^5$, which may generate a significant volume decrease since all of the normal velocities may become negative due to the relatively small strain energy density and the free boundary thus moves inwardly. The interval which bounds the Lagrange multiplier is halved and the Lagrange multiplier is given by

$$\ell = (\ell_1 + \ell_2)/2 \quad (38)$$

from which the normal velocities v_n in (36) as well as the extension velocities, which will be discussed later, can

be determined and thus the generalized expansion coefficients $\boldsymbol{\alpha}$ in (26) can be updated. Since the implicit level set function $\Phi(\mathbf{x}, t + \tau)$ in (21) and the material volume $V(\Phi)$ in (5) can also be determined, the value of the volume constraint function $G(\Phi)$ in (29) will be finally obtained. Therefore, either the lower bound ℓ_1 or the upper bound ℓ_2 can be updated and the interval which bounds the Lagrange multiplier can be repeatedly halved until its size is less than the convergence criteria. It should be noted that the present algorithm does not assume that the volume is constant during the iterations, but the volume constraint can be exactly satisfied based on the geometry at time $t + \tau$. As noted in [Sigmund (2001)], a bi-sectioning algorithm is usually effective with a fast convergence speed.

By using this bi-sectioning algorithm, the material volume constraint can be exactly satisfied during the iterations and thus the material volume can be constant during the evolution of the moving free boundary. Hence, the present normal velocities may become a kind of mass conserving velocities and the present level set method can be regarded as mass conservative.

4.5 Shape Optimization

According to the present steepest gradient method, for the optimal design, we have

$$v_n = \boldsymbol{\varepsilon}^T \mathbf{C} \boldsymbol{\varepsilon} - \ell = 0 \quad (39)$$

which implies that the strain energy density ($\boldsymbol{\varepsilon}^T \mathbf{C} \boldsymbol{\varepsilon}$) is constant everywhere along the optimal free boundary Γ_M since the Lagrange multiplier ℓ is time-dependent only. It should be noted that this can also be the objective of the classical shape optimization methods based on a shape sensitivity analysis [(Rozvany, 1998); Sokolowski and Zolesio (1992)]. In the classical shape optimization, a key concept is the ‘‘speed function’’ V_n of the optimality condition associated with a small variation in the boundary shape in the normal direction n , similar to the present normal velocity v_n . In general, it is necessary that

$$V_n(\mathbf{x}) = 0 \quad (40)$$

everywhere on the design boundary of the optimal structure. Physically, this indicates that the mutual energy form of the elastic structure reaches a constant value on the boundary [Sokolowski and Zolesio (1992)]. Hence, the present level set model can perform not only the free

boundary-based topology optimization but also the classical shape optimization.

In most shape optimization applications, a Lagrangian formulation of boundary propagation was used to achieve the optimality condition and obtain an optimal shape of the structure [Rozvany (1998); Sokolowski and Zolesio (1992)]. Only an explicit boundary representation method is used and the boundary changes can be accomplished only if the connectivity of the boundaries does not change since there is a severe limitation that only a structure of a fixed topology can be optimized. In the present level set-based optimization model, both shape and topology can be optimized simultaneously. The whole design domain is implicitly represented by a level set function $\Phi(\mathbf{x})$ and the moving free boundary is represented by the zero level sets, which may experience significant topological changes such as developing sharp corners, breaking apart, merging together or even disappearing. Furthermore, topological changes in a structure can be captured, rather than tracked [Osher and Fedkiw (2002)]. Hence, the present level set-based optimization method can be more powerful than the classical shape optimization methods.

4.6 Extension Velocities

As aforementioned, the normal velocity v_n defined at the free boundary must be extended, either to the whole design domain D [Allaire, Jouve, and Toader (2004)] or to a narrow band around the free boundary [Osher and Fedkiw (2002)], in the Eulerian type level set methods. The choice of an extension velocity method is crucial since it can directly influence the overall efficiency of the level set method [Richards, Bloomfield, Sen, and Calea (2001); Wang and Wang (2005c); Wang and Wang (2005d)].

In the present study, a physically meaningful extension velocity method without the additional PDE solving procedure is presented for structural shape and topology optimization. According to Eq. (36), a natural extension of the normal velocity v_n at the free boundary can be obtained if the strain field $\boldsymbol{\varepsilon}(\mathbf{u})$ is extended to the entire design domain D by assuming $\boldsymbol{\varepsilon}(\mathbf{u}) = 0, \mathbf{u} \in (D \setminus \Omega)$. Nevertheless, this extension will introduce an apparent discontinuity in the extension velocity at the free boundary since the strain field is not continuous across the free boundary. To avoid the numerical instabilities and to guarantee a smooth progress of the free boundary,

this discontinuity should be eliminated. Hence, a linear smoothing filter is introduced in the narrowband region around the free boundary, which is defined as

$$\Xi = \left\{ \mathbf{x} \in \mathbb{R}^d \mid |\Phi(\mathbf{x})| \leq \Delta \right\} \quad (41)$$

where Δ is the bandwidth. The extension velocity v_n^e in the narrowband is smoothed as \widehat{v}_n^e by using a simple linear filter (radially linear ‘hat’ kernel popular in the SIMP-based topology optimization [Sigmund (2001); Bendsøe and Sigmund (2003)]) to achieve an excellent smoothing effect [Wang and Wang (2005a); Wang and Wang (2005c)], which can be written as

$$\widehat{v}_n^e(\mathbf{x}) = k^{-1}(\mathbf{x}) \sum_{\mathbf{p} \in N(\mathbf{x})} W_c(\|\mathbf{p} - \mathbf{x}\|) v_n^e(\mathbf{x}) \quad (42)$$

where

$$W(\|\mathbf{p} - \mathbf{x}\|) = r_{\min} - \|\mathbf{p} - \mathbf{x}\| \quad (43)$$

$$k(\mathbf{x}) = \sum_{\mathbf{p} \in N(\mathbf{x})} W(\|\mathbf{p} - \mathbf{x}\|) \quad (44)$$

in which $N(\mathbf{x})$ is the neighborhood of $\mathbf{x} \in \Xi$ in the filter window and r_{\min} the window size. It should be noted that the present smoothing operation is quite similar to the sensitivity filtering in the popular element-based SIMP method for structural topology optimization [Bendsøe and Sigmund (2003)], which is used to eliminate the numerical instabilities effectively. Hence, a direct link between the present boundary-based shape and topology optimization method and the popular element-based topology optimization method can be established by taking the present normal velocity as the sensitivity in the SIMP method. It can thus be expected that the present extension velocity method can also eliminate the numerical instabilities effectively. Different from the SIMP method, the present method only smoothes out the velocity in the neighborhood of the free boundary since it is a boundary-based method.

Finally, the overall extension velocity can be obtained as

$$v_n^e = v_n^e(\mathbf{x}) = \begin{cases} \boldsymbol{\varepsilon}^T \mathbf{C} \boldsymbol{\varepsilon} - \ell & \mathbf{x} \in \mathbb{R}^d \mid \Phi(\mathbf{x}) < -\Delta \\ \widehat{v}_n^e(\mathbf{x}) & \mathbf{x} \in \Xi \\ -\ell & \mathbf{x} \in \mathbb{R}^d \mid \Phi(\mathbf{x}) > \Delta \end{cases} \quad (45)$$

Using this extension velocity field v_n^e , $\mathbf{B}(\boldsymbol{\alpha})$ can be obtained from Eq. (25) at each time step and thus the generalized expansion coefficients $\boldsymbol{\alpha}$ in (26) can be updated.

The motion of the free boundary can be produced by using the updated implicit level set function $\Phi(\mathbf{x}, t)$ in (21). This procedure should be repeated until the convergence criteria have been reached. Theoretically, when an optimal solution is reached, the extension velocities inside the material domain will be

$$v_n^e = v_n^e(\mathbf{x}) = 0, \quad \mathbf{x} \in \Omega \quad (46)$$

Hence, the strain energy density field, as well as the stress distribution, is theoretically homogeneous inside the material domain of the optimal structure, according to Eq. (45). Therefore, in the present shape and topology optimization, theoretically, an optimal structure is achieved when the strain energy distribution inside the material domain and along the free boundary is homogeneous.

Therefore, the resulting extension velocities are physically meaningful since both the strain energy density and the mass-conserving Lagrange multiplier are closely associated with physics. In the present shape and topology optimization, materials which are not used efficiently such that the strain energy density is too small can be indicated by the extension velocity field with multiple valleys at the undesired locations. As illustrated in the present numerical examples, the evolution of the level set function with this extension velocity field may finally lead to the creation of a new hole inside the material domain, similar to the evolutionary structural optimization approach [Xie and Steven (1993)], the bubble method [Eschenauer, Kobelev, and Schumacher (1994)], and the topological gradient method [Burger, Hackl, and Ring (2004)]. This can be a significant improvement over the conventional level set methods, which only allow limited topological changes by splitting or merging connected components [Burger (2004)]. Furthermore, due to the RBF implicit modeling and the linear smoothing filtering, the smoothness of the implicit level set function can be well maintained during the time advancement without reinitialization.

5 Numerical Examples and Discussion

In this section, numerical examples in two dimensions are presented to illustrate the performance and success of the present method for structural shape and topology optimization. Unless stated otherwise, all the units are consistent and the following parameters are assumed as: the Young’s elasticity modulus $E = 1$ for solid materials, $E = 1 \times 10^{-5}$ for void materials, and Poisson’s ra-

tio $\nu = 0.3$. The implicit level set function $\Phi(\mathbf{x})$ is initially chosen as a signed distance function by using the present RBF modeling from a set of given points and no extra efforts such as reinitialization are made to keep this property during the optimization process.

For all examples, a fixed rectilinear mesh is specified over the entire design domain for finite element (FE) analysis of the structures. The FE analysis is based on the bilinear rectangular elements and an “ersatz material” approach, which is well-known in topology optimization that can be rigorously justified in some cases [Allaire (2001); Allaire, Jouve, and Toader (2004)]. In numerical practice of the “ersatz material” approach, material density is assumed to be piecewise constant in each element and is adequately interpolated in those elements cut by the zero level set function (the free boundary). It is also assumed that the knots of the RBFs are coincidental to the nodes of the rectilinear mesh. Furthermore, $\Delta = 1$ grid size for the bandwidth size, $r_{\min} = 1.2$ grid size for the filter window size. The present algorithm is terminated when the relative difference between two successive objective function values is less than 10^{-5} or when the given maximum number of iterations has been reached. The topologies are given in black-and-white form based on the scalar value of the implicit function $\Phi(\mathbf{x})$, as defined in Eq. (1). All the CPU time is based on a desktop computer under the MATLAB environment with an Intel Pentium IV processor of 3.00 GHz clock speed.

5.1 Short Cantilever Beam

The minimum compliance design problem of a short cantilever beam is shown in Fig. 3. The whole design domain D is a rectangle of size 2×1 with a fixed boundary ∂D (zero displacement boundary condition) on the left side and a unit vertical point load $P = 1$ applied at a fixed non-homogeneous Neumann boundary ∂D_N , the middle point of the right side. The specified material volume fraction is $\zeta = 0.5$. The distribution of the RBF knots shown in Fig. 3 is for illustrative purposes only since different meshes may be adopted for this example. It should correspond to the actual nodes distribution of the underlying FE mesh for structural analysis.

Figure 4 displays the evolution history of an optimal topology of the short cantilever beam with an initial design as shown in Fig. 4(a) by using the present level set method with a 60×30 FE mesh with a time step size of

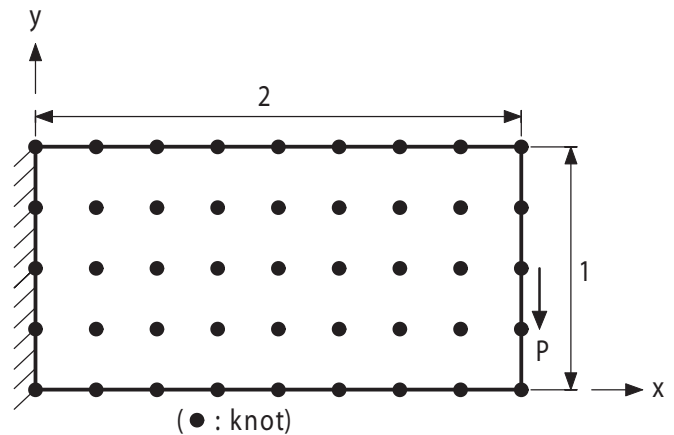


Figure 3 : Definition of the minimum compliance design problem of a short cantilever beam.

$\tau = 0.01$ and a free shape parameter of $c = 0.1$. It can be seen that significant topological changes have been achieved and the final design as shown in Fig. 4(f) is similar to those reported in the literature [Allaire, Jouve, and Toader (2004); Allaire, Gournay, Jouve, and Toader (2004); Wang and Wang (2005c)] using the conventional level set methods. Hence, optimal topologies can also be obtained by solving the ODEs in Eq. (24) using the present method, rather than the PDEs using the upwind schemes in the conventional level set methods [Sethian (1999); Osher and Fedkiw (2002)]. The evolution of the corresponding moving free boundary Γ_M is shown in Fig. 5, in which the free boundary is approximately depicted by piecewise lines and the extension velocities at each knot are indicated by the arrows. Using the present extension velocities, the moving free boundary can develop sharp corners, break apart, merge together and disappear in an automatic manner during the course of evolution. Although the maximum velocity is located on the free boundary in the initial design, as shown in Fig. 5(a), the location is rapidly shifted to around the fixed boundary ∂D . Hence, in the majority of the design domain, the extension velocities will approach to zero to reach a homogeneous distribution of the stress distribution, as theoretically predicted. In the optimal solution, as shown in Fig. 6, the scalar normal velocities at the free boundary, as well as in most of the material domain, become almost zero, which agrees well with the theoretical prediction [Allaire, Jouve, and Toader (2004)] and indicates that the

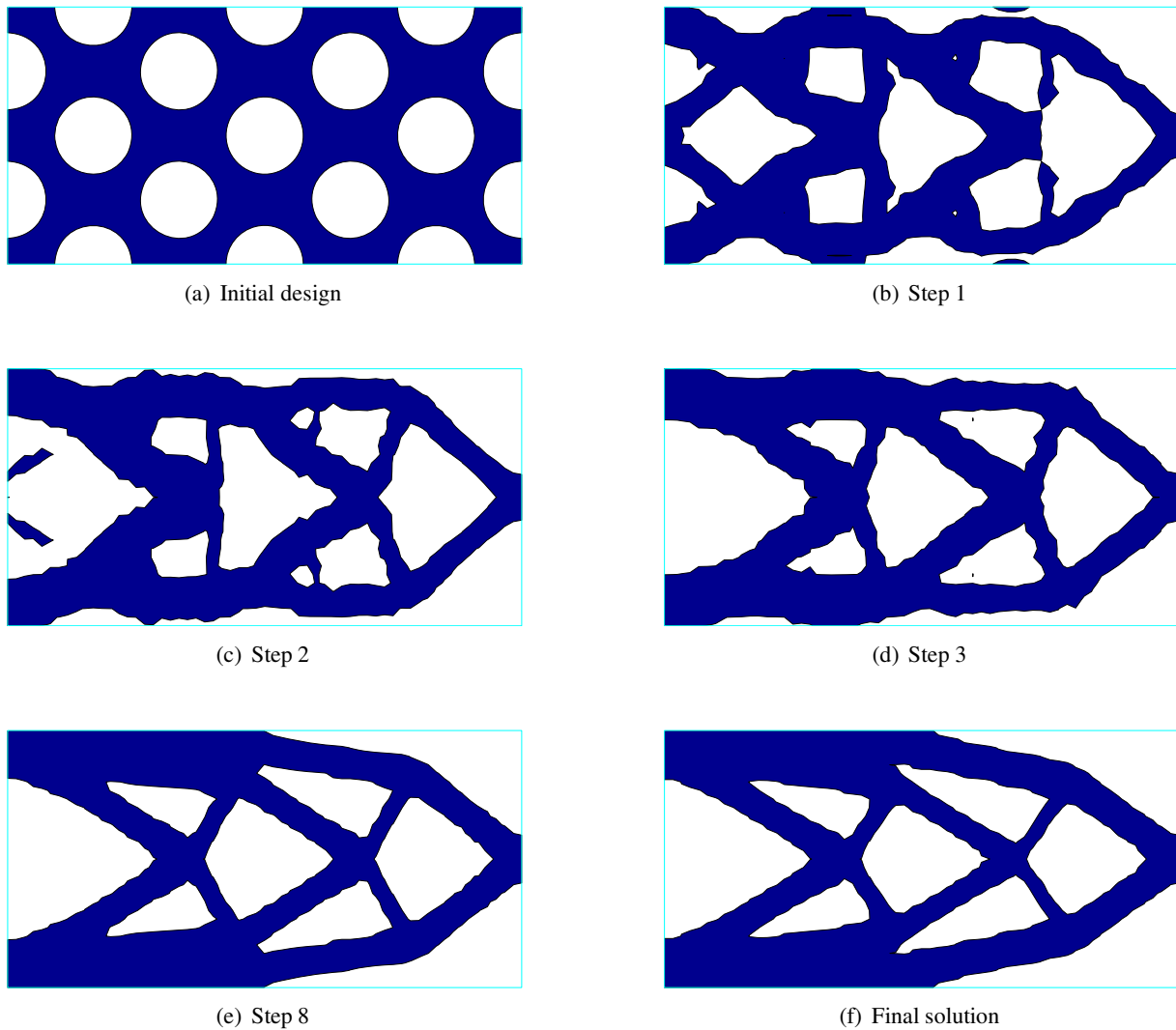


Figure 4 : Evolution of an optimal solution for the short cantilever beam.

shape and topology optimization is achieved. The high velocity distribution around parts of the the fixed boundary ∂D and the fixed non-homogeneous Neumann boundary ∂D_N is due to the local effects of the applied force, according to Saint-Venant's principal [Choi and Horgan (1977)], and cannot be totally eliminated by performing a shape and topology optimization. As a further demonstration, Figure 7 displays the evolution history of the strain energy density field in the design domain. It can be seen that the apparent inhomogeneous distribution of the strain energy density of the initial design can be quickly eliminated during the iterations by the present shape and topology optimization and a nearly homogeneous distribution can be achieved in the final solution, as theoret-

cally predicted.

Figure 8 shows the convergence speed of the objective function and the volume function for the short cantilever beam. It can be seen that the compliance of the optimal solution is significantly better than that of the initial design and the compliance converges rapidly due to the present level set-based optimization method. The optimal topology is not changed after step 8, as shown in Fig. 4 and thus the subsequent iterations are mainly performed to achieve an optimal shape. It can be seen from Fig. 8(a) that the subsequent improvement in the objective function is almost negligible compared with the significant improvement in those iterations to perform a topology optimization. However, making more efforts to

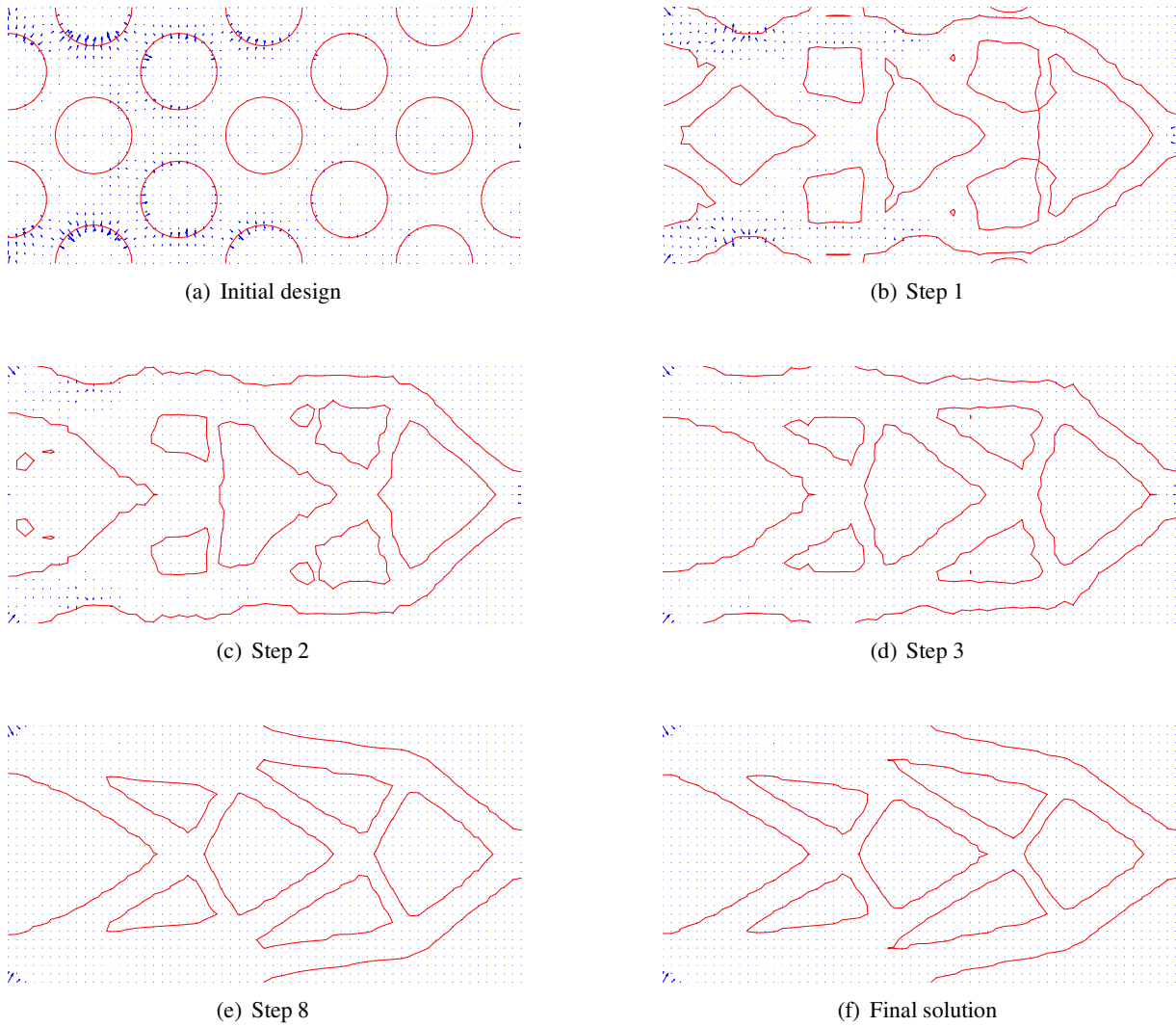


Figure 5 : Evolution of the moving free boundary of the short cantilever beam.

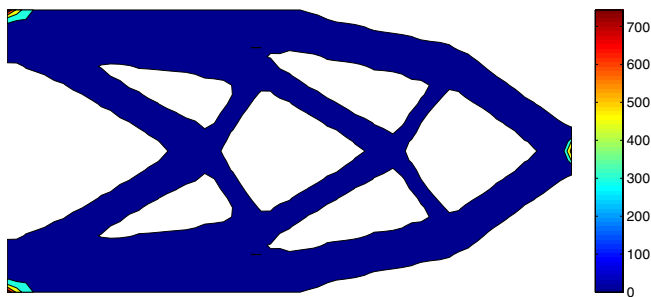


Figure 6 : Scalar extension velocity field ($v_n^e \geq 0$) for an optimal solution of the short cantilever beam.

perform shape optimization is worthwhile and indispensable. As shown in Fig. 7, shape optimization can reduce the magnitude of the maximum strain energy density and arrive at an almost homogeneous distribution of the stress field at the free boundary and inside the material domain, as aforementioned. Furthermore, it can be seen from Fig. 8(b) that the equal volume constraint ($V/V_0 = 0.5$) can be exactly satisfied during the course of evolution, though the initial design possesses a higher material volume ($V/V_0 = 0.578$) and is thus infeasible. As aforementioned, in the present study this is achieved by choosing an appropriate Lagrange multiplier using a bi-sectioning algorithm, rather than based on the problematic assumption that the material volume can keep unchanged during

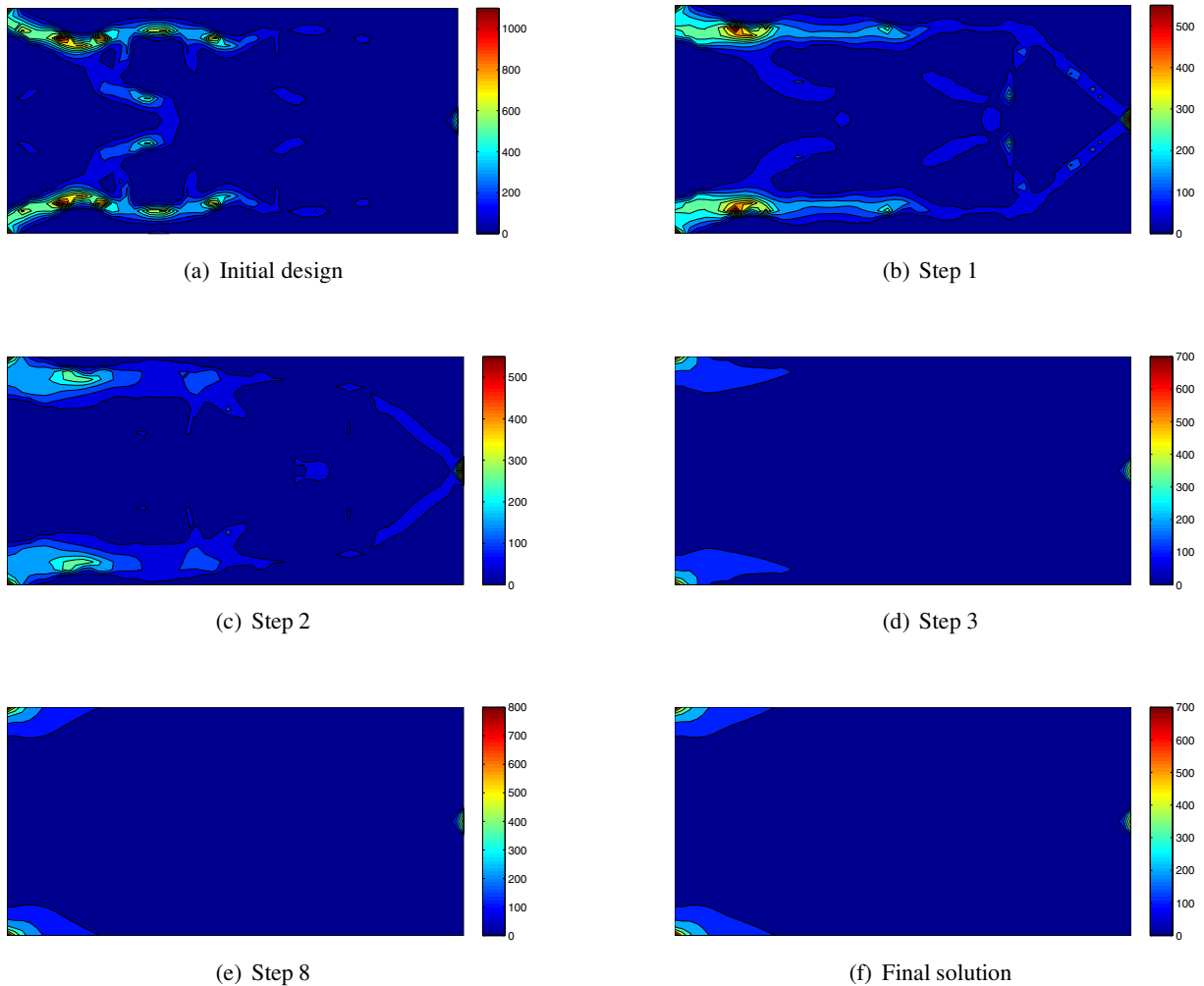


Figure 7 : Evolution of the strain energy density field of the short cantilever beam.

the evolution [Osher and Santosa (2001); Wang, Wang, and Guo (2003); Wang and Wang (2005d)]. Hence, the optimal solutions can be guaranteed to be feasible and the present level set method may become mass conservative to make the material volume constant during the iterations. Furthermore, it can be inferred that those conventional level set methods for shape and topology optimization [Osher and Santosa (2001); Wang, Wang, and Guo (2003); Allaire, Jouve, and Toader (2004); Wang and Wang (2004b); Wang and Wang (2004a); Wang and Wang (2005b); Wang and Wang (2005c)] may also become mass conservative if the present mass-conserving velocities are adopted.

For the purpose of comparison, this shape and topology optimization problem is solved again by using a conven-

tional level set model in [Mitchell (2004)] and the present mass-conserving extension velocities. In the level set model, a second-order ENO (essentially non-oscillatory) upwind scheme is used for the propagation of the free boundary and a third-order reinitialization algorithm is adopted to minimize the numerical diffusion around the location of the original interface [Tsai and Osher (2003)], and an aggressive CFL number of 1 is used to drive a fast convergence. Reinitialization as an auxiliary step is performed every 5 times of transport and the maximum number of iterations is specified as 200. The final solutions are shown in Fig. 9. It can be seen that the final topology is similar to the optimal topology shown in Fig. 4(f), however, the optimization is not converged within 200 iterations since there is an apparent discrepancy between the free boundary shown in Fig. 9(a) and the zero

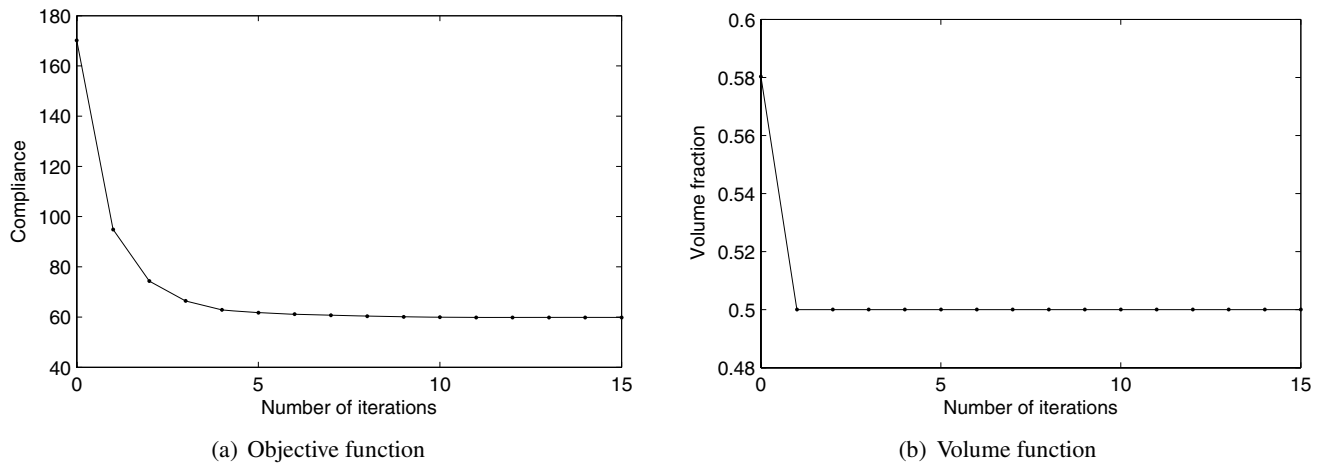


Figure 8 : Convergence of the objective function and the volume function for the short cantilever beam.

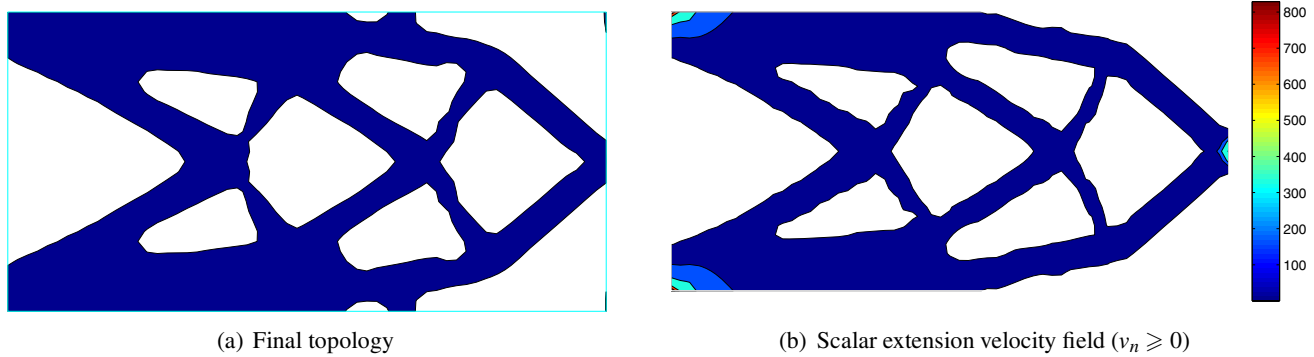


Figure 9 : Final solutions for the short cantilever beam using a conventional level set method.

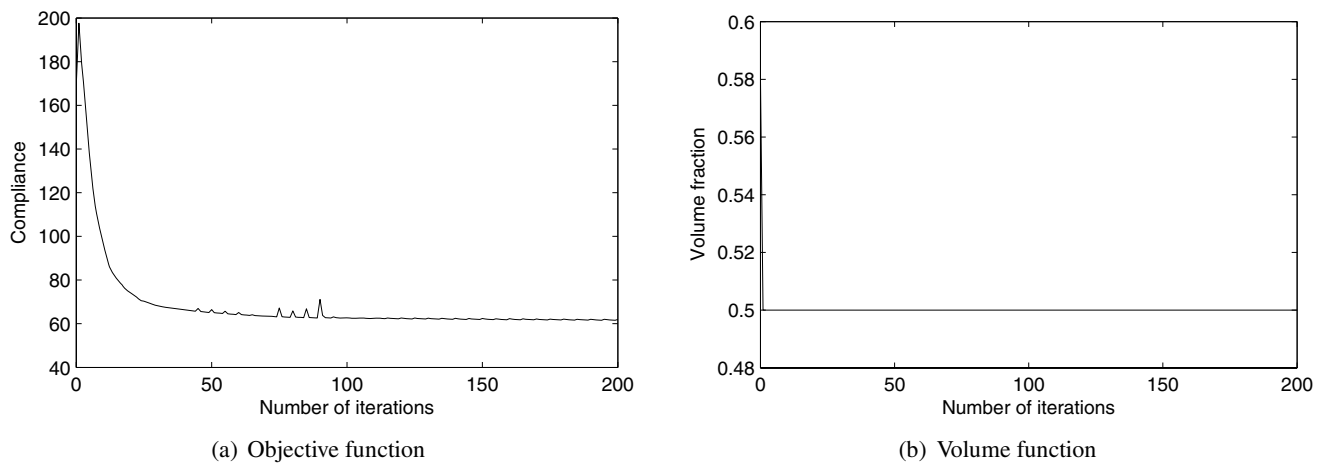


Figure 10 : Convergence of the objective function and the volume for the short cantilever beam using a conventional level set method.

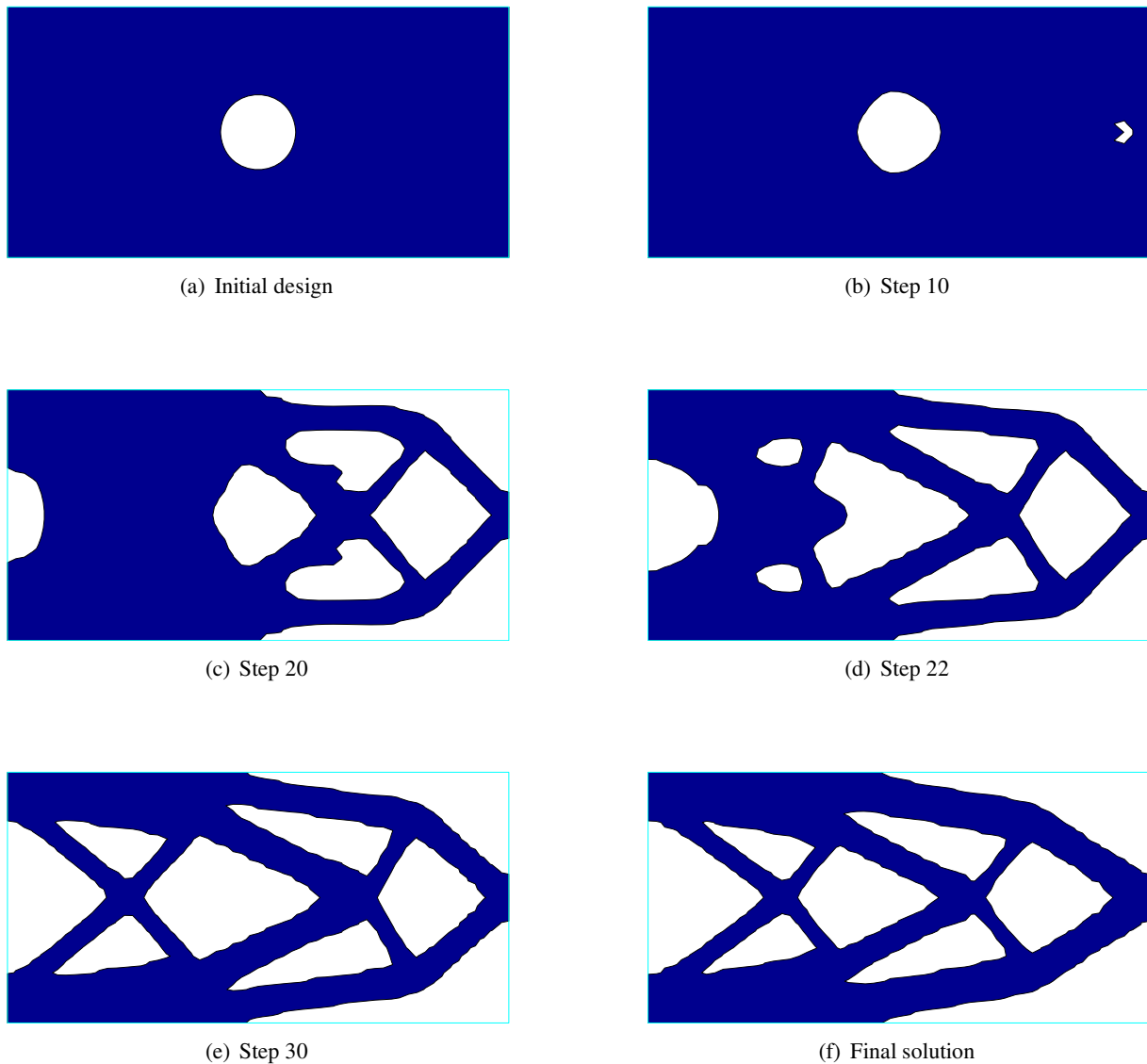


Figure 11 : Evolution of an optimal solution using an initial design with a central hole.

scalar velocity curve shown in Fig. 9(b). The convergence speed of the objective function and the material volume is shown in Fig. 10. As expected, due to the use of the present mass conserving velocities, the material volume shown in Fig. 10(b) is nearly constant during the iterations. Nevertheless, the objective function shown in Fig. 10(a) using the conventional level set method decreases in a not quite stable way due to the use of an aggressive CFL number, furthermore, it converges in a significantly slower speed than using the present level set method as shown in Fig. 8(a). This is a typical drawback of a CFL-dependent conventional level set model

using an explicit time integration scheme, as aforementioned. On the other hand, the present level set method converges rapidly since it is a CFL-free method and time-stable for all knot distributions [Schaback and Wendland (2001)]. Hence, the present method may significantly excel the conventional CFL-dependent level set methods in convergence speed.

Nucleation of some new holes in the material domain can be observed in Figs. 4(b) and 4(c), which suggests that the present level set method has the capability of nucleation of new holes due to the absence of reinitialization. To further demonstrate this capability and the

flexibility of the present method, the shape and topology optimization is performed again starting from a design with one single hole, as shown in Fig. 11(a). Since its material volume fraction of 0.9649 is too higher than the required volume fraction of 0.5, the initial design is quite far away from the feasible domain. In this case, although the present method may still be able to satisfy the volume constraint at each iteration, it may experience significant difficulties and numerical instabilities to handle topological changes to achieve a drastic volume reduction within one single step. To drive the evolution of the optimal solution from the infeasible domain to the feasible one smoothly, a minor modification to the present mass-conserving Lagrange multiplier is here presented by combining the present method with the method in [Allaire, Jouve, and Toader (2004); Wang and Wang (2005d)] using a fixed Lagrange multiplier to decrease the material volume. A neighborhood of the feasible domain is defined first. For this example, a volume fraction range of $[0.4, 0.6]$ for the pre-specified volume fraction of 0.5 is used as the neighborhood. When the material volume fraction falls inside this range, the variable Lagrange multiplier ℓ is determined by the present bi-sectioning algorithm as aforementioned. However, when the material volume fraction falls outside this range, a fixed Lagrange multiplier ($\ell = 20$ for this example) is used to drive the convergence of the material volume fraction towards the neighborhood of the feasible domain in a stable and smooth manner. With this enhancement, the present method becomes more flexible to deal with this kind of special problems.

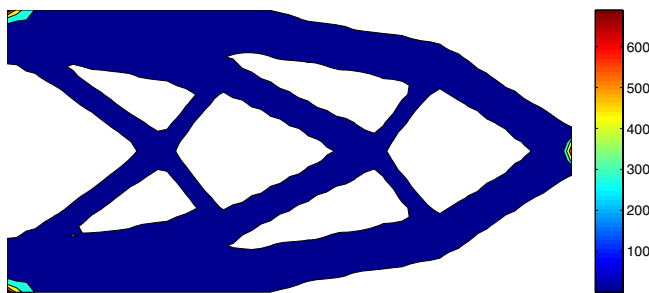


Figure 12 : Scalar extension velocity field ($v_n^e \geq 0$) for an optimal solution using an initial design with a central hole.

The corresponding shape and topology optimization is again performed and the initial design, the intermediate

results and the final solution are shown in Fig. 11. It can be seen that drastic topological changes have been achieved in a stable way and the final solution is quite similar to the one shown in Fig. 4(f), in which an initial design with more holes than those of the optimal design is used. Furthermore, the final scalar extension velocity field shown in Fig. 12 is also quite similar to the one shown in Fig. 6. Hence, the capability of nucleation of new holes and the relative insensitivity of the final solutions to the initial designs are clearly demonstrated. Because of this capability, the final solution is less sensitive to the initial designs. Furthermore, Figure 13 shows that the convergence of both the objective function and the volume constraint function from the initial infeasible domain to the feasible domain are reached after step 24. The infeasible initial design quite far away from the feasible domain is driven successfully towards the feasible domain by using the present method. It should be noted that the compliance increases with time before reaching the feasible domain since the initial design possesses a much lower compliance value of 41.1345 than that of the optimal solution (60.4013) due to its much higher initial material volume than required. As noted by [Wang and Wang (2005c)], using a fixed Lagrange multiplier can only guarantee the decrease of an unconstrained objective function combining the compliance function with the volume function. However, a relatively large Lagrange multiplier can be used to guarantee the decrease of the volume function due to the monotonousness of the volume function, as previously discussed. After step 24, the optimization is performed in the feasible domain and a variable Lagrange multiplier can be used. The capability of nucleation of new holes inside the material domain is further demonstrated in Fig. 14, in which an initial design without a hole evolves into an optimal topology with a few holes, similar to the optimal solution shown in Fig. 4(f). Since the initial volume fraction of 0.5 can satisfy the volume constraint, a further modification to the Lagrange multiplier should not be performed here. Again, the insensitivity to the initial designs is also illustrated.

In the conventional level set methods, the nucleation of new holes is not allowed for and thus a bubble or topological gradient method has to be incorporated to achieve a less initial design-dependent optimal design, as shown in [Eschenauer, Kobelev, and Schumacher (1994); Burger, Hackl, and Ring (2004); Allaire, Gournay, Jouve, and Toader (2004)]. Since both the topological and shape

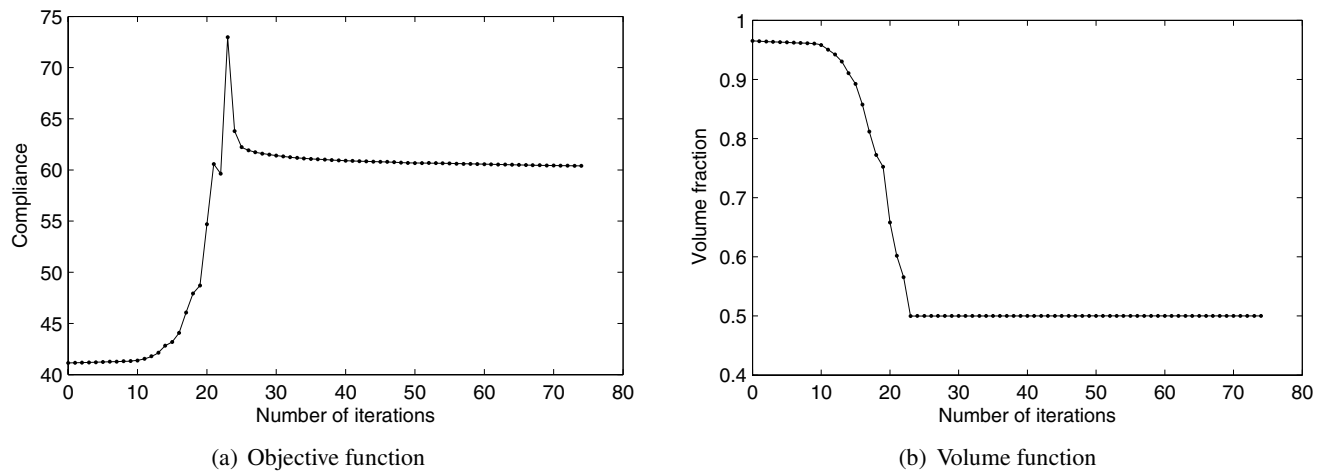


Figure 13 : Convergence of the objective function and the volume for the short cantilever beam using an initial design with a central hole.

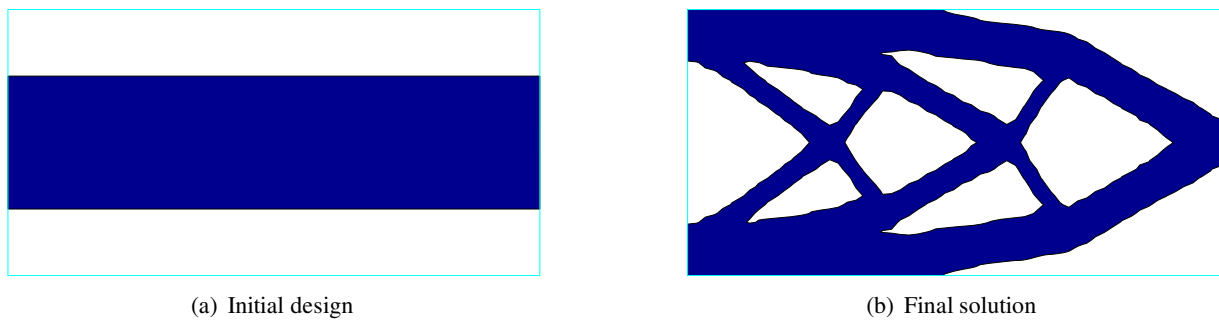


Figure 14 : Optimal solution using an initial design without a hole.

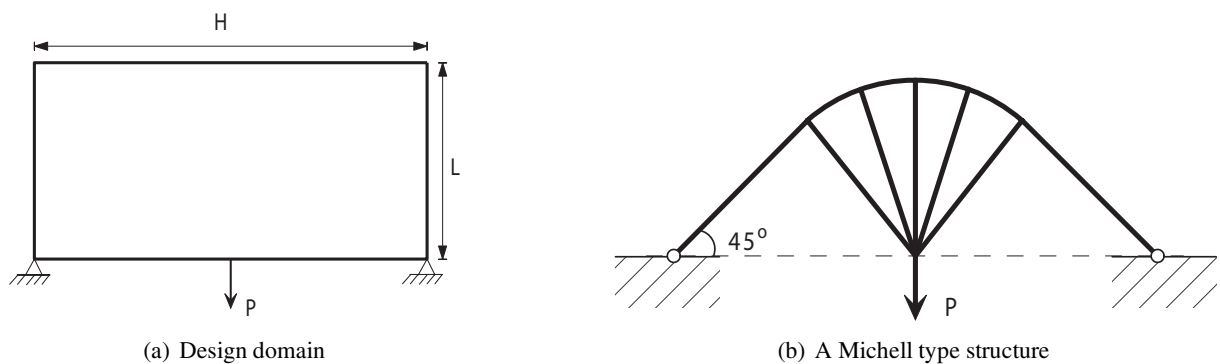


Figure 15 : Optimal design problem for Michell type structures with fixed supports.

derivatives are used in a modified level set method, it would be quite difficult to switch between them in an automatic way [Burger, Hackl, and Ring (2004); Allaire, Gournay, Jouve, and Toader (2004)]. In the present method, the topological derivative is not used and the cre-

ation of new holes can be automatically realized by using the shape derivatives and the present mass conserving extension velocities with the absence of reinitialization.

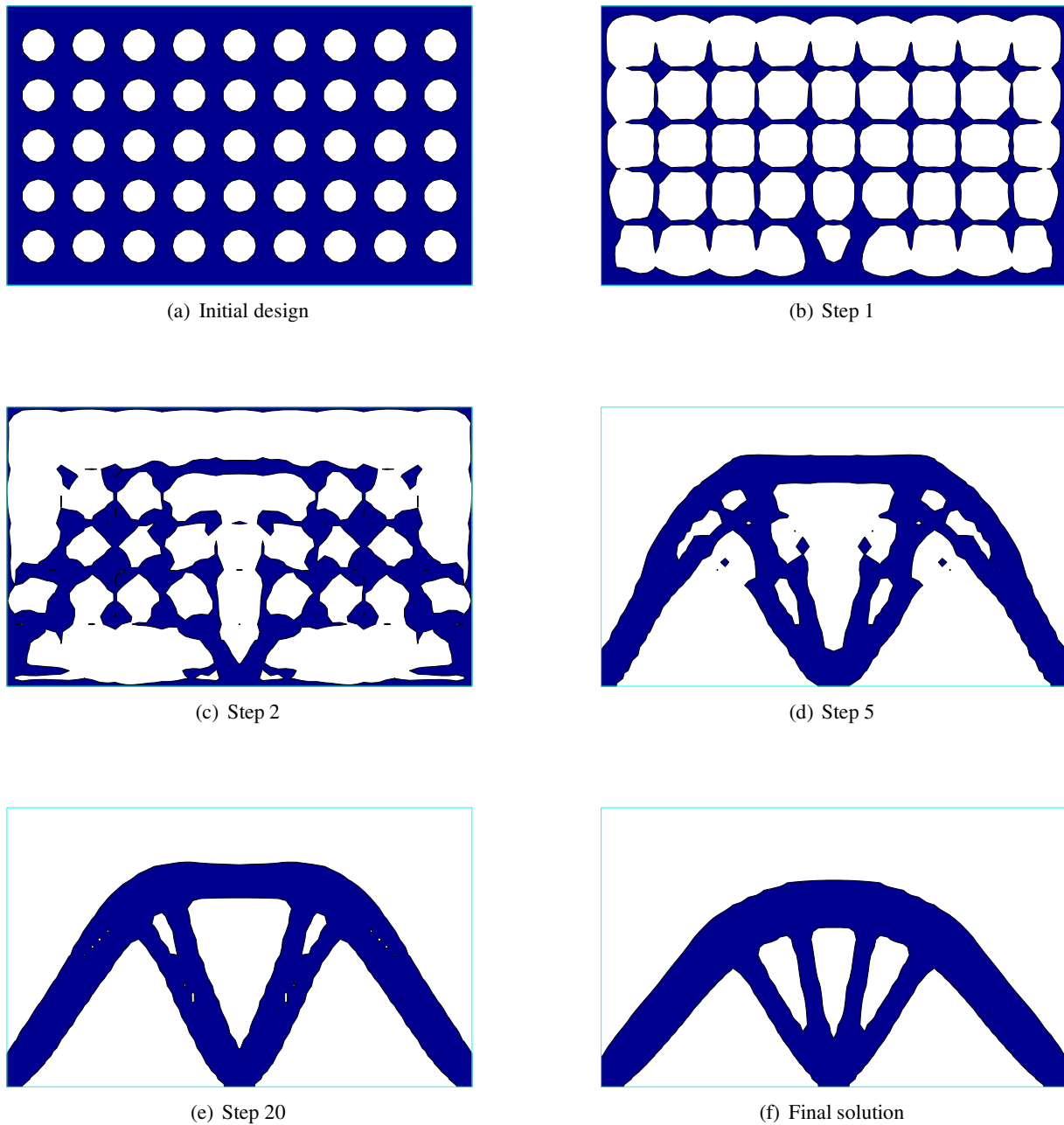


Figure 16 : Evolution of an optimal solution for the Michell type structure.

5.2 Michell Type Structure

The present level set method is finally applied to the classical Michell type structure problem, in which a theoretical Michell's solution is available in the literature [Michell (1904); Hemp (1973); Xie and Steven (1993); Wang and Tai (2005)], as shown in Fig. 15(b). The whole design domain D is a rectangle of size $L \times H$, the two bottom corners have the pinned supports, and a unit ver-

tical point force P is applied at the middle point of the bottom side. As shown in Figure 15(b), the theoretical optimum topology consists of two 45° arms extending from the supports towards an approximately 90° central fan section which extends upwards from the point of application of the force. In the present study, it is assumed that $L = 2$, $H = 1.2$, $P = 1$, and a pre-specified material volume fraction $\zeta = 0.3$. The domain D is discretized

with a fixed rectangular mesh of 60×36 and a time step size of $\tau = 0.01$ together with a free shape parameter of $c = 0.001$ is adopted.

A heavily perforated structure as shown in Fig. 16(a) is chosen as the initial design. The present level set method without modifying the Lagrange multiplier as just suggested is applied to demonstrate its efficiency and accuracy in dealing with heavily perforated structures as initial designs. The corresponding evolution history of the shape and topology is shown in Fig. 16. Significant topological changes due to the elimination of internal holes have been obtained. The final topology consisting of two arms and a central fan section is quite similar to the theoretical optimum topology shown in Fig. 15(b) and therefore the effectiveness and accuracy of the present level set method is again verified. Furthermore, a shape optimization is also performed simultaneously in the present method and thus an optimal boundary shape can be obtained in the final solution, as shown in Figs. 16(f) and 17, in which the zero scalar velocity curve corresponds to the free boundary of the final solution almost exactly. Hence, the present optimization method can be more powerful than the traditional topology optimization methods [Michell (1904); Bendsøe and Kikuchi (1988); Bendsøe (1989); Xie and Steven (1993); Wang and Tai (2005)]. For this problem, although the initial material volume fraction of 0.7023 is significantly larger than the required volume fraction of 0.3, the present method without further modifying the Lagrange multiplier is thus still applicable. For this case, using a problem-dependent fixed Lagrange multiplier, which may cause mathematical complexity in determining its appropriate value, to drive the material volume towards the feasible domain, as previously suggested, is not needed. The convergence of the objective function and the volume constraint function is shown in Fig. 18. Although the objective function may increase in the early iterations due to the large number of bars to be broken to satisfy the volume constraint, as shown in Fig. 16, it finally converges in a smooth and stable way. Again, as expected, Fig. 18(b) displays that the volume constraint can be exactly satisfied during the course of evolution.

The effect of support type on the final design is shown in Fig. 19. The support of this problem is changed to be simply supported as shown in Fig. 19(a). Without changing any other parameters, the shape and topology optimization is performed again using the present method

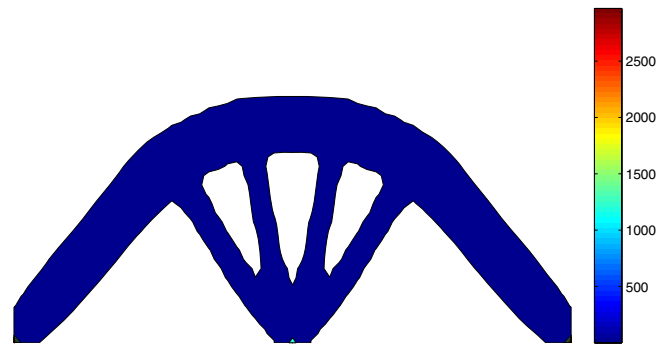


Figure 17 : Scalar extension velocity field ($v_n^e \geq 0$) for an optimal solution of the Michell type structure.

and the final solution is shown in Fig. 19(b), in which a less rigid pin-like connection near the supports is suggested for the final truss-like structure. Comparing Fig. 16(f) with Fig. 19(b), it can be seen that the support type can influence the optimal topology significantly. This is consistent with the conclusions made in [Bendsøe and Sigmund (2003)] based on the element-based SIMP method for structural topology optimization.

6 Conclusions

A level set approach based on the implicit free boundary parametrization method is successfully developed for structural shape and topology optimization. The implicit level set function is represented and approximated by using the RBF implicit modeling with IMQ splines. Because of the global smoothness and the exponential convergence rate of the IMQs, a high level of accuracy and smoothness of the implicit function is achieved. Furthermore, by assuming that the time dependence of the implicit function is due to the generalized expansion coefficients of the RBF interpolant, the Hamilton-Jacobi PDE is converted into a mathematically more convenient coupled ODE and the original time dependent initial value problem is changed to a relatively simple time-dependent interpolation problem for the initial values of the generalized expansion coefficients, which can be solved by using a collocation formulation of the method of lines. The resulting system of non-linear coupled ODEs can be solved by lots of existing ODE solvers. The time integration of the ODEs can be CFL-free because of the positive definiteness of the IMQs.

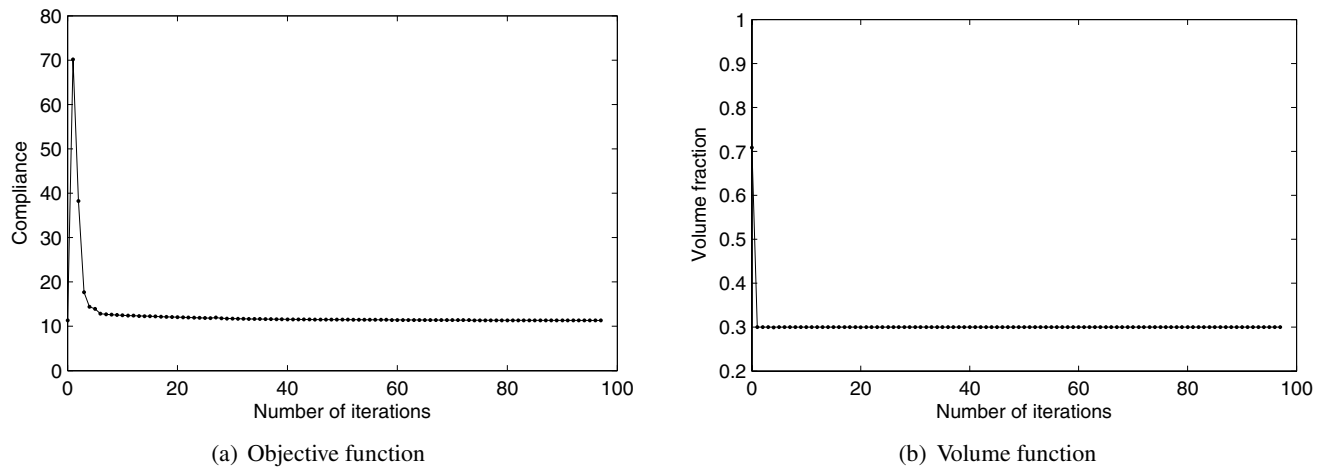


Figure 18 : Convergence of the objective function and the volume function for the Michell type structure.

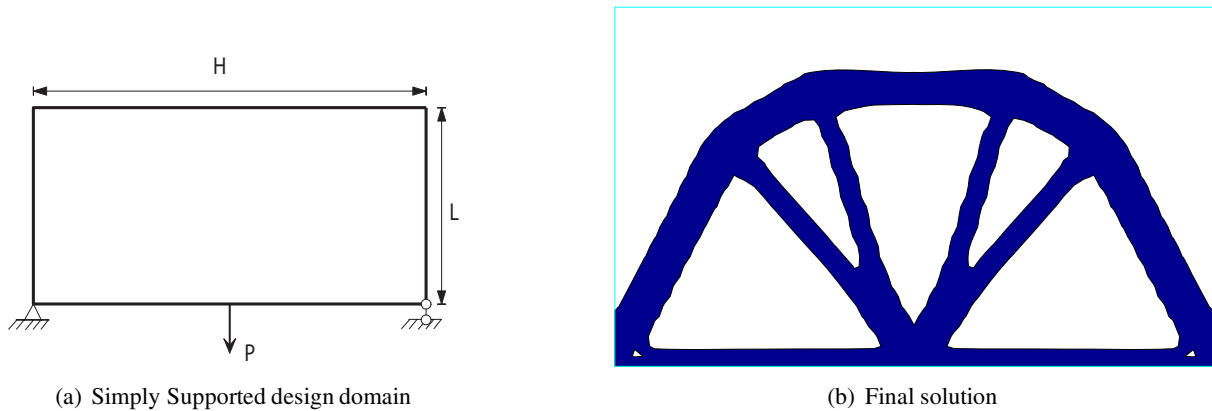


Figure 19 : Effect of the support type on the final solution.

The present extended level set method is then applied to a classical shape and topology optimization problem. The proposed shape and topology optimization process operates on the implicit scalar level set function represented by the RBF implicit modeling and uses a steepest gradient method to find the decent direction of the normal velocity for the minimization of an objective function. By using the present bi-sectioning algorithm, the Lagrange multiplier can be accurately obtained and the resulting normal velocity becomes mass conserving and the present extended level set method can thus be mass conservative. It is also found that the classical shape optimization can be performed during the course of evolution. By using the global strain energy density field and a linear smoothing filter, the normal velocity at the free boundary is naturally and smoothly extended to the

whole design domain D without using an additional PDE solving procedure. Moreover, reinitialization of the implicit level set function is eliminated to allow for the nucleation of new holes in the material domain.

This proposed method is implemented in the framework of shape and topological optimum of minimum compliance design and its higher efficiency and accuracy over the conventional level set methods are illustrated. Numerical examples of 2D structures are chosen to show the success of the present method in accuracy, convergence speed and insensitivity to initial designs. Compared with the conventional level set methods, the present method can generate similar optimal designs without the numerically more complicated PDE solving procedures and without the significant time step constraint due to the CFL condition and exactly satisfy the volume con-

straint during the iterations to guarantee that the final design be feasible and, furthermore, it can largely eliminate the dependency on initial designs due to its capability in the nucleation of new holes. It is also highlighted that the efforts in shape optimization is worthwhile and indispensable since an almost homogeneous strain energy density distribution can be achieved. It is suggested that the introduction of the radial basis functions to the conventional level set methods possesses promising potentials in structural shape and topology optimization.

Acknowledgement: This research work is partly supported by the Research Grants Council of Hong Kong SAR (Project No. CUHK4164/03E), a Post-doctoral Fellowship from the Chinese University of Hong Kong (No. 04/ENG/1), the Natural Science Foundation of China (NSFC) (Grants No. 50128503 and No. 50390063), and a Research Fellowship from the National University of Singapore, which the authors gratefully acknowledge.

References

- Akin, J. E.; Arjona-Baez, J.** (2001): Enhancing structural topology optimization. *Engineering Computations*, vol. 18, no. 3–4, pp. 663–675.
- Allaire, G.** (2001): *Shape Optimization by the Homogenization Method*. Springer, New York.
- Allaire, G.; Gournay, F. D.; Jouve, F.; Toader, A.-M.** (2004): Structural optimization using topological and shape sensitivity via a level set method. Internal report 555, Ecole Polytechnique, France, 2004.
- Allaire, G.; Jouve, F.; Toader, A.-M.** (2004): Structural optimization using sensitivity analysis and a level-set method. *Journal of Computational Physics*, vol. 194, pp. 363–393.
- Atluri, S. N.; Shen, S. P.** (2002): *The meshless local Petrov-Galerkin (MLPG) method*. Tech. Science Press, Forsyth, GA.
- Belytschko, T.; Black, T.** (1999): Elastic crack growth in finite elements with minimal remeshing. *International Journal for Numerical Methods in Engineering*, vol. 45, no. 5, pp. 601–620.
- Belytschko, T.; Xiao, S. P.; Parimi, C.** (2003): Topology optimization with implicit functions and regularization. *International Journal for Numerical Methods in Engineering*, vol. 57, no. 8, pp. 1177–1196.
- Bendsøe, M. P.** (1989): Optimal shape design as a material distribution problem. *Structural Optimization*, vol. 1, pp. 193–202.
- Bendsøe, M. P.; Kikuchi, N.** (1988): Generating optimal topologies in structural design using a homogenization method. *Computer Methods in Applied Mechanics and Engineering*, vol. 71, pp. 197–224.
- Bendsøe, M. P.; Sigmund, O.** (2003): *Topology Optimization: Theory, Methods and Applications*. Springer-Verlag, Berlin.
- Buhmann, M. D.** (2004): *Radial Basis Functions: Theory and Implementations*, volume 12 of *Cambridge Monographs on Applied and Computational Mathematics*. Cambridge University Press, New York, NY.
- Burger, M.** (2004): Lecture notes on infinite-dimensional optimization and optimal design. Report 285J, University of California, Los Angeles, CA, USA, 2004.
- Burger, M.; Hackl, B.; Ring, W.** (2004): Incorporating topological derivatives into level set methods. *Journal of Computational Physics*, vol. 194, pp. 344–362.
- Carr, J. C.; Beatson, R. K.; Cherrie, J. B.; Mitchell, T. J.; Fright, W. R.; McCallum, B. C.; Evans, T. R.** (2001): Reconstruction and representation of 3D objects with radial basis functions. In *ACM SIGGRAPH 2001*, pp. 67–76, Los Angeles, CA.
- Cecil, T.; Qian, J. L.; Osher, S.** (2004): Numerical methods for high dimensional Hamilton-Jacobi equations using radial basis functions. *Journal of Computational Physics*, vol. 196, no. 1, pp. 327–347.
- Cheng, A.-D.; Golberg, M. A.; Kansa, E. J.; Zammito, G.** (2003): Exponential convergence and H-c multiquadric collocation method for partial differential equations. *Numerical Methods for Partial Equations*, vol. 19, no. 5, pp. 571–594.
- Choi, I.; Horgan, C. O.** (1977): Saint Venant's principle and end effects in anisotropic elasticity. *Journal of Applied Mechanics*, vol. 44, pp. 420–430.

- Crandall, M. G.; Lions, P. L.** (1984): Two approximations of solutions of Hamilton-Jacobi equations. *Mathematics of Computation*, vol. 43, pp. 1–19.
- Enright, D.; Losasso, F.; Fedkiw, R.** (2005): A fast and accurate semi-Lagrangian particle level set method. *Computers & Structures*, vol. 83, no. 6–7, pp. 479–490.
- Eschenauer, H. A.; Kobelev, V. V.; Schumacher, A.** (1994): Bubble method for topology and shape optimization of structures. *Structural Optimization*, vol. 8, no. 1, pp. 42–51.
- Franke, R.** (1982): Scattered data interpolation: Tests of some methods. *Mathematics of Computation*, vol. 38, pp. 181–200.
- Gómez, P.; Hernández, J.; López, J.** (2005): On the reinitialization procedure in a narrow-band locally refined level set method for interfacial flows. *International Journal for Numerical Methods in Engineering*, in press.
- Greenberg, M. D.** (1998): *Advanced Engineering Mathematics*. Prentice-hall International, Inc., Upper Saddle River, New Jersey, USA, 2nd edition.
- Greengard, L.; Rokhlin, V.** (1987): A fast algorithm for particle simulations. *Journal of Computational Physics*, vol. 73, pp. 325–348.
- Hardy, R. L.** (1990): Theory and applications of the multiquadric-biharmonic method: 20 years of discovery. *Computers & Mathematics with Applications*, vol. 19, no. 8/9, pp. 163–208.
- Hemp, W. S.** (1973): Michell's structural continua. In *Optimum Structures*, chapter 4. Clarendon Press, Oxford.
- Jiang, G.-S.; Peng, D.** (2000): Weighted ENO schemes for Hamilton-Jacobi equations. *SIAM Journal on Scientific Computing*, vol. 21, pp. 2126–2143.
- Kansa, E. J.** (1990): Multiquadrics-A scattered data approximation scheme with applications to computational fluid dynamics: I. Surface approximations and partial derivative estimates. *Computers and Mathematics with Applications*, vol. 19, pp. 127–145.
- Kansa, E. J.; Powerb, H.; Fasshauerc, G. E.; Ling, L.** (2004): A volumetric integral radial basis function method for time-dependent partial differential equations. I. Formulation. *Engineering Analysis with Boundary Elements*, vol. 28, pp. 1191–1206.
- Lageneste, L. D. D.; Pitsch, H.** (2002): A numerical scheme for the large-eddy simulation of turbulent combustion using a level-set method. Annual research briefs, Center for Turbulence Research, Stanford University, Standford, CA, USA, 2002.
- Madsen, N. K.** (1975): The method of lines for the numerical solution of partial differential equations. *ACM SIGNUM Newsletter*, vol. 10, no. 4, pp. 5–7.
- Michell, A. G. M.** (1904): The limits of economy of material in frame-structures. *Philosophical Magazine*, vol. 8, no. 6, pp. 589–597.
- Mitchell, I. M.** (2004): A toolbox of level set methods. Tech. Rep. TR-2004-09, Department of Computer Science, University of British Columbia, Canada, 2004.
- Morse, B. S.; Yoo, T. S.; Chen, D. T.; Rheingans, P.; Subramanian, K. R.** (2001): Interpolating implicit surfaces from scattered surface data using compactly supported radial basis functions. In *SMI '01: Proceedings of the International Conference on Shape Modeling & Applications*, pp. 89–98, Washington, DC, USA. IEEE Computer Society.
- Norato, J.; Haber, R.; Tortorelli, D.; Bendsøe, M. P.** (2004): A geometry projection method for shape optimization. *International Journal for Numerical Methods in Engineering*, vol. 60, no. 14, pp. 2289–2312.
- Osher, S.; Fedkiw, R. P.** (2001): Level set methods: An overview and some recent results. *Journal of Computational Physics*, vol. 169, pp. 463–502.
- Osher, S.; Santosa, F.** (2001): Level-set methods for optimization problems involving geometry and constraints: Frequencies of a two-density inhomogeneous drum. *Journal of Computational Physics*, vol. 171, pp. 272–288.
- Osher, S.; Sethian, J. A.** (1988): Front propagating with curvature dependent speed: Algorithms based on Hamilton-Jacobi formulations. *Journal of Computational Physics*, vol. 78, pp. 12–49.
- Osher, S.; Shu, C.-W.** (1991): High-order essentially nonoscillatory schemes for Hamilton-Jacobi equations.

- SIAM Journal on Numerical Analysis*, vol. 28, pp. 907–922.
- Osher, S. J.; Fedkiw, R. P.** (2002): *Level Set Methods and Dynamic Implicit Surfaces*. Springer-Verlag, New York.
- Peng, D.; Merriman, B.; Osher, S.; Zhao, H.; Kang, M.** (1999): A PDE-based fast local level set method. *Journal of Computational Physics*, vol. 155, pp. 410–438.
- Platte, R. B.; Driscoll, T. A.** (2005): Eigenvalue stability of radial basis function discretizations for time-dependent problems. Technical Report 2005–01, Department of Mathematical Sciences, University of Delaware, USA, 2005.
- Richards, D. F.; Bloomfield, M. O.; Sen, S.; Calea, T. S.** (2001): Extension velocities for level set based surface profile evolution. *Journal of Vacuum Science and Technology A*, vol. 19, no. 4, pp. 1630–1635.
- Rozvany, G.** (1998): *Structural Design via Optimality Criteria*. Kluwer, Dordrecht.
- Rozvany, G. I. N.** (2001): Aims, scope, methods, history and unified terminology of computer-aided topology optimization in structural mechanics. *Structural and Multidisciplinary Optimization*, vol. 21, no. 2, pp. 90–108.
- Rozvany, G. I. N.; Zhou, M.; Birker, T.** (1992): Generalized shape optimization without homogenization. *Structural Optimization*, vol. 4, pp. 250–254.
- Schaback, R.; Wendland, H.** (2001): Characterization and construction of radial basis functions. In Dyn, N.; Leviatan, D.; Levin, D.; Pinkus, A.(Eds): *Multivariate approximation and applications*, pp. 1–24. Cambridge University Press, Cambridge, UK.
- Sethian, J. A.** (1999): *Level Set Methods and Fast Marching Methods*. Cambridge Monographs on Applied and Computational Mathematics. Cambridge University Press, Cambridge, UK, 2nd edition.
- Sethian, J. A.; Wiegmann, A.** (2000): Structural boundary design via level set and immersed interface methods. *Journal of Computational Physics*, vol. 163, no. 2, pp. 489–528.
- Sigmund, O.** (2001): A 99 line topology optimization code written in MATLAB. *Structural and Multidisciplinary Optimization*, vol. 21, no. 2, pp. 120–127.
- Sokolowski, J.; Zolesio, J.** (1992): Introduction to shape optimization: shape sensitivity analysis. In *Springer Series in Computational Mathematics*, volume 10. Springer, Berlin, Germany.
- Strouboulis, T.; Copps, K.; Babuska, I.** (2001): The generalized finite element method. *Computer Methods in Applied Mechanics and Engineering*, vol. 190, pp. 4081–4193.
- Sussman, M.; Fatemi, E.** (1999): An efficient, interface-preserving level set re-distancing algorithm and its application to interfacial incompressible fluid flow. *SIAM Journal on Scientific Computing*, vol. 20, pp. 1165–1191.
- Tanskanen, P.** (2002): The evolutionary structural optimization method: theoretical aspects. *Computer Methods in Applied Mechanics and Engineering*, vol. 191, no. 47-48, pp. 5485–5498.
- Tsai, R.; Osher, S.** (2003): Level set methods and their applications in image science. *Communications in Mathematical Sciences*, vol. 1, no. 4, pp. 623–656.
- Vese, L. A.; Chan, T. F.** (2002): A multiphase level set framework for image segmentation using the mumford and shah model. *International Journal of Computer Vision*, vol. 50, pp. 271–293.
- Wang, M. Y.; Wang, S. Y.** (2005): Bilateral filtering for structural topology optimization. *International Journal for Numerical Methods in Engineering*, vol. 63, no. 13, pp. 1911–1938.
- Wang, M. Y.; Wang, X.** (2004): PDE-driven level sets, shape sensitivity and curvature flow for structural topology optimization. *CMES: Computer Modeling in Engineering & Sciences*, vol. 6, no. 4, pp. 373–395.
- Wang, M. Y.; Wang, X.** (2005): A level-set based variational method for design and optimization of heterogeneous objects. *Computer-Aided Design*, vol. 37, pp. 321–337.
- Wang, M. Y.; Wang, X.; Guo, D.** (2003): A level set method for structural topology optimization. *Com-*

puter Methods in Applied Mechanics and Engineering, vol. 192, pp. 227–246.

Wang, M. Y.; Wang, X. M. (2004): “Color” level sets: A multi-phase method for structural topology optimization with multiple materials. *Computer Methods in Applied Mechanics and Engineering*, vol. 193, no. 6–8, pp. 469–496.

Wang, S. Y.; Tai, K. (2004): Graph representation for evolutionary structural topology optimization. *Computers & Structures*, vol. 82, no. 20–21, pp. 1609–1622.

Wang, S. Y.; Tai, K. (2005): Bar-system representation method for structural topology optimization using the genetic algorithms. *Engineering Computations*, vol. 22, no. 2, pp. 206–231.

Wang, S. Y.; Tai, K.; Wang, M. Y. (2006): An enhanced genetic algorithm for structural topology optimization. *International Journal for Numerical Methods in Engineering*, vol. 65, no. 1, pp. 18–44.

Wang, S. Y.; Wang, M. Y. (2005): A moving superimposed finite element method for structural topology optimization. *International Journal for Numerical Methods in Engineering*, in press.

Wang, S. Y.; Wang, M. Y. (2005): Radial basis functions and level set method for structural topology optimization. *International Journal for Numerical Methods in Engineering*, in press.

Wang, X.; Mei, Y.; Wang, M. Y. (2004): Incorporating topology/phase derivatives into level set methods for optimization of solids. In *WISDOM 2004-Warsaw International Seminar on Design and Optimal Modeling*, Warsaw, Poland.

Xia, Q.; Wang, M. Y.; Wang, S. Y.; Chen, S. K. (2005): Semi-lagrangian method for level-set based structural topology and shape optimization. *Structural and Multidisciplinary Optimization*, accepted.

Xie, Y. M.; Steven, G. P. (1993): A simple evolutionary procedure for structural optimization. *Computers & Structures*, vol. 49, no. 5, pp. 885–896.

Ye, J. C.; Bresler, Y.; Moulin, P. (2002): A self-referencing level-set method for image reconstruction from sparse Fourier samples. *International Journal of Computer Vision*, vol. 50, no. 3, pp. 253–270.

